iScience

Article

# Tissue origin of endothelial cells determines immune system modulation and regulation of HIF-1α-, TGF-β-, and VEGF signaling

## Graphical abstract

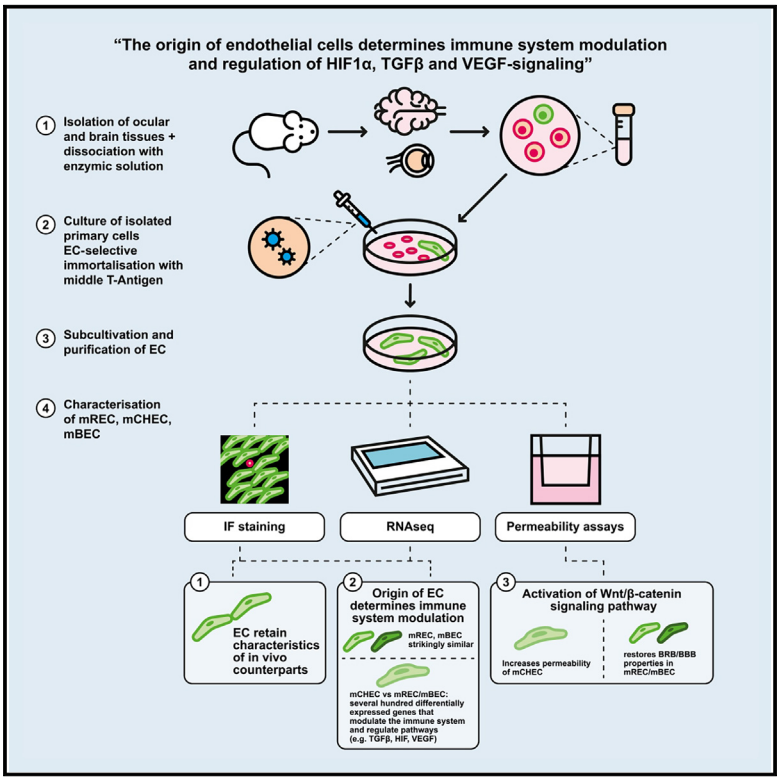


## Highlights

- Novel models of endothelial cells (EC) of different tissue origin
- Signaling pathway regulation and immune response varies depending on origin of ECs
- Transcriptome data indicate tissue-specific susceptibility of EC in DR and nAMD
- Barrier function can be restored upon Wnt/β-catenin activation

## Authors

Robin Heiden, Laura Hannig, Jakob S. Bernhard, ..., Andreas Neueder, Carola Y. Förster, Barbara M. Braunger

## Correspondence

foerster_c@ukw.de (C.Y.F.), b.braunger@uke.de (B.M.B.)

## In brief

Molecular biology; Cell biology

Heiden et al., 2025, iScience *28*, 111740
February 21, 2025 
https://doi.org/10.1016/j.isci.2024.111740

CellPress

iScience

CellPress
OPEN ACCESS

Article

# Tissue origin of endothelial cells determines immune system modulation and regulation of HIF-1α-, TGF-β-, and VEGF signaling

Robin Heiden,[1,6] Laura Hannig,[1,5,6] Jakob S. Bernhard,[1,6] Mario Vallon,[1] Anja Schlecht,[1,5] Nico Hofmann,[1] Süleyman Ergün,[1] Franziska Hoschek,[2] Maximilian Wagner,[2] Andreas Neueder,[2,4] Carola Y. Förster,[3,*] and Barbara M. Braunger[1,5,7,*]

[1]Institute of Anatomy and Cell Biology, University of Würzburg, 97070 Würzburg, Germany
[2]Department of Neurology, Ulm University Hospital, 89081 Ulm, Germany
[3]Department of Anaesthesiology, Intensive Care, Emergency and Pain Medicine, University Hospital of Würzburg, 97080 Würzburg, Germany
[4]Center for Molecular Neurobiology Hamburg, University Medical Center Hamburg-Eppendorf, 20246 Hamburg, Germany
[5]Institute of Neuroanatomy, University Medical Center Hamburg-Eppendorf, 20246 Hamburg, Germany
[6]These authors contributed equally
[7]Lead contact
*Correspondence: foerster_c@ukw.de (C.Y.F.), b.braunger@uke.de (B.M.B.)
https://doi.org/10.1016/j.isci.2024.111740

## SUMMARY

Tight junctions of vascular endothelial cells in the central nervous system form the blood-brain and inner blood-retinal barriers, the integrity of which are further influenced by neighboring cells such as pericytes, astrocytes/Müller glial processes, and immune cells. In addition, the retina is shielded from the fenestrated endothelium of the choriocapillaris by the epithelial barrier of the retinal pigment epithelium. Dysfunction of the blood retinal barriers and/or proliferation of retinal and choroidal endothelial cells are caused by late stages of diabetic retinopathy (DR) and neovascular age-related macular degeneration (nAMD), the main causes of blindness in western countries. To elucidate endothelial-derived pathomechanisms in DR and nAMD, we established immortalized mouse cell lines of retinal and choroidal endothelial cells and immortalized brain endothelial cells as CNS-derived controls. We then used immunofluorescence staining, state-of-the-art long-range RNA sequencing and monolayer permeability assays to compare the functional state of these cells depending on their tissue origin. We furthermore demonstrate that activation of the wingless-type MMTV integration site (Wnt)/β-catenin signaling pathway restored blood brain/retinal barrier properties in brain and retinal endothelial cells, but unexpectedly increased permeability of choroidal endothelial cells. Transcriptome profiling showed that depending on the tissue origin of endothelial cells, regulation of the immune system was altered and pathways such as hypoxia-inducible factor (HIF)-1/2α, transforming growth factor (TGF)-β, and vascular endothelial growth factor (VEGF) were differentially regulated, strongly indicating their contribution in the molecular pathogenesis of DR and nAMD. These findings significantly increase the understanding of the vascular biology of endothelial cells, highlighting the fact that depending on their tissue origin, their contribution to vascular pathologies varies.

## INTRODUCTION

Vascular endothelial cells of the brain and retina form the blood-brain barrier (BBB) and inner blood-retinal barrier (iBRB), respectively, through tight junctions to shield the neuronal tissue from harmful blood-derived molecules.[1–3] However, these barriers are highly specialized multicellular structures, with pericytes, embedded in the capillary basement membrane, astrocyte/Müller glia processes, and immune cells further contributing to their integrity.[2,3] The retina is furthermore shielded from the fenestrated endothelium of the choriocapillaris through a second, epithelial barrier that is formed through tight junctions of the retinal pigment epithelium (RPE) and termed as outer BRB.[1,2]

Diseases such as diabetic retinopathy (DR) and age-related macular degeneration (AMD) are both associated with a breakdown of the BRB and leading causes of blindness in developed countries.[4–7] High blood glucose levels are the main cause for DR development, which is characterized by alterations in retinal blood vessels such as microaneurysm formation and breakdown of the iBRB leading to edema and hemorrhage.[5,7] Eventually, DR progresses to a proliferative stage in which retinal neovascularization occurs. These newly formed blood vessels protrude into the retina and vitreous body, are highly leaky, and prone to hemorrhage.[5] AMD is considered a multifactorial disease and characterized by accumulation of extracellular deposits (drusen) underneath the retinal pigment epithelium

(RPE).[4] Eventually, with disease progression, drusen-induced tissue damage leads to inflammation and proliferation of choroidal vessels into the subretinal space (choroidal neovascularization), a hallmark of wet AMD.[4] If untreated, wet AMD rapidly results in macular edema, hemorrhage, degeneration of photoreceptors, and central vision loss. Thus, in their late, proliferative stages, both conditions (DR and neovascular AMD) are associated with a breakdown of the blood retinal barriers and vascular proliferation.

To elucidate the pathomechanisms of DR and AMD, different knockout and transgenic mice have been used.[8–11] However, cell cultures of retinal or choroidal endothelial cells would be valuable tools to study molecular pathways of disease *in vitro*, as well as, for example, allow to conduct high-throughput drug discovery screens. So far, successful isolation and culture of primary retinal and choroidal endothelial cells have only been described for bovine and human starting material.[12–16] Murine primary retinal and choroidal endothelial cells are highly resistant to culturing and expansion.

To circumvent these problems, we adapted a protocol for immortalization of murine brain and myocardial endothelial cells[15,17–20] to immortalization of mouse retinal and choroidal endothelial cells. The polyoma virus middle T antigen was used to selectively immortalize endothelial cells in primary cultures of mouse retinal or choroidal cells. Immunofluorescence staining and third generation long-range RNA sequencing (nanopore RNA sequencing) analyses showed that the cells retained essential characteristics of their *in vivo* counterparts. Furthermore, functional analyses showed that barrier properties of the individual cell cultures could be modulated using wingless-type MMTV integration site (WNT)/β-catenin activation. Nanopore RNA sequencing demonstrated a very similar transcriptional profile of retinal and brain endothelial cells but identified 493 differentially expressed genes between choroidal endothelial cells and retinal/brain endothelial cells. Gene ontology analyses indicated predominant transcriptional differences, depending on the origin of tissue the endothelial cells derive from, in the activation of the immune system or cells such as microglia/macrophages and differences in the regulation of pathways such as hypoxia-inducible factor (HIF)-1/2α-, transforming growth factor (TGF)-β-, and vascular endothelial growth factor (VEGF) signaling.

## RESULTS

### Generation of *in vitro* models of murine retinal, choroidal, and brain endothelial cells

First, we established primary cultures from enzymatically dissociated retinae, choroids and brain tissue isolated from juvenile mice (Figures 1A and S1A). We isolated and processed brain endothelial cells side-by-side, using essentially the same and previously published protocol,[18,21–23] to confirm central nervous system (CNS) characteristics of the isolated retinal endothelial cells and non-CNS characteristics of the isolated choroidal endothelial cells (Figures 1A, S1A, and S1B).

Our dissociation protocol and culture conditions favored survival of stromal cells. As the retina and brain are mainly composed of neurons and glia, only very few cells survived culturing. In contrast, primary cultures from stroma-rich choroids were much denser and included pigmented cells (e.g., melanocytes and/or retinal pigment epithelial cells) (Figure S1A). Twenty-four h and 48 h after establishing primary cultures, the cells were transduced with a retrovirus encoding the polyoma virus middle T antigen. The middle T antigen mediates selective immortalization of endothelial cells.[24] Consequently, the primary cultures gradually developed into endothelial monocultures as the transformed endothelial cells grew faster than other cell types and cell divisions were not restricted by the Hayflick limit anymore. Depending on the tissue, immortalized endothelial cell clones became visible by day 3 (retina) or by day 15 (choroid) or day 5 (brain) (Figures S1A and S1B). By day 21–25 the cultures appeared homogenous in phase contrast microscopy. However, double immunofluorescence staining in cultures from the stroma-rich choroid on day 45 for the endothelial marker platelet endothelial cell adhesion molecule 1 (PECAM1 and CD31) and the non-endothelial, stromal cell marker α2-actin (ACTA2), detected some residual contaminating ACTA2-positive cells, i.e., pericytes, vascular smooth muscle cells, and/or fibroblasts (Figure S1C). By day 60, all cells in culture stained positive for PECAM1/CD31, indicating that endothelial cells had completely outgrown other cell types (Figure 1B). Immortalized retinal endothelial cell monocultures were termed REC, choroidal endothelial cell monocultures ChEC, and brain endothelial monocultures BEC.

We analyzed the transcriptomes of the generated cell lines (REC, BEC, and ChEC) using nanopore long-range, third generation RNA sequencing (https://nanoporetech.com) for in depth characterization of the established cell cultures. Long-range sequencing offers several key advantages, one of them being the absolute determination of transcript sequences and thus unambiguous quantification of expression changes. To further confirm the purity of the established immortalized cell cultures, we extracted the normalized counts of endothelial and non-endothelial markers from the transcriptomic data. By doing so, we demonstrated a robust expression of several endothelial markers (Figure 1C). Non-endothelial, stromal markers were either undetectable or had a very low expression in all three endothelial cell lines, further confirming their endothelial identity and the purity of the cells (Figure 1C). Moreover, we validated these results using immunohistochemical staining for the tight junction marker CLDN5 (Figure S2A), whose expression correlates well with barrier function in the CNS *in vivo*.[25] Accordingly, CLDN5 showed higher expression in REC vs. ChEC (Figures S2A and S2C). In contrast, the expression of plasmalemma vesicle associated protein (PLVAP), which represents a marker for fenestrated endothelial cells *in vivo*[8,26,27] (Figures S2D–S2F) and tight junction protein1 (TJP1/ZO1, Figures S2G–S2I) did not show remarkable differences between the individual cell lines, most likely due to their immortalization and *in vitro* culturing of the cells.

### In-depth transcriptomic characterization of REC, ChEC, and BEC

Most noticeable, the nanopore RNA sequencing showed a very high similarity between REC and BEC, with only 21 differentially expressed genes (out of 24,469 detected genes in total), strongly indicating the very close similarity of retinal and brain endothelial

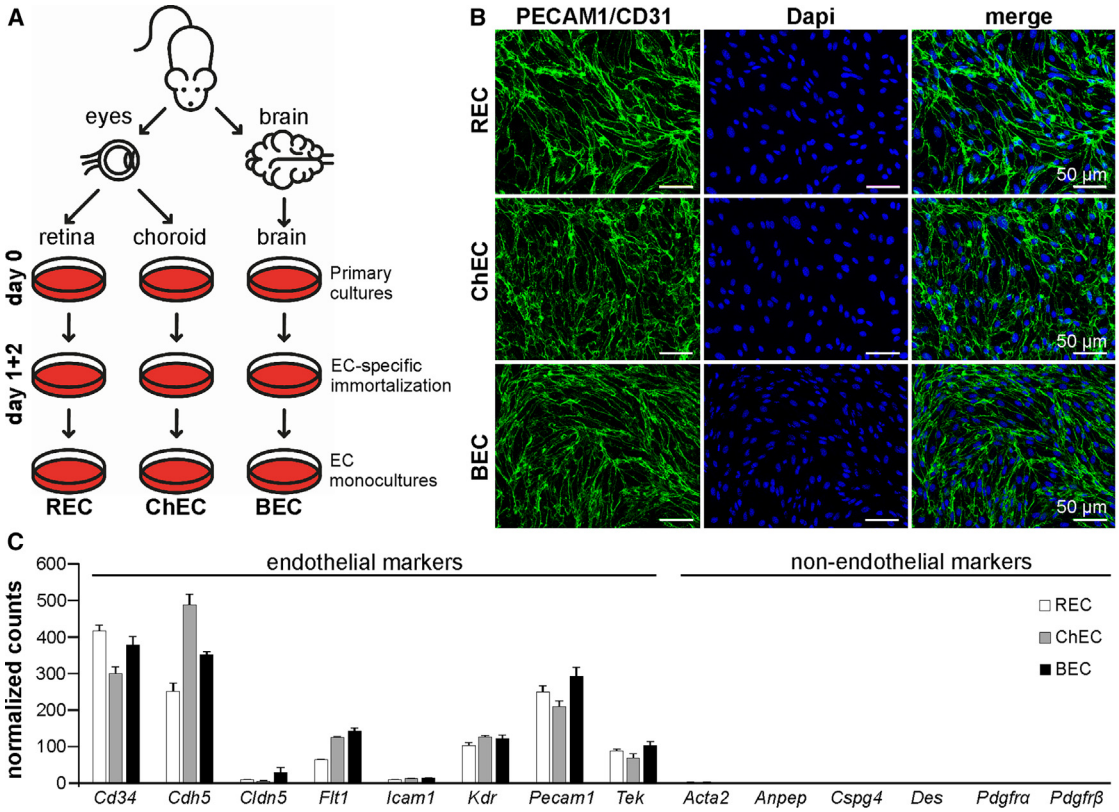


**Figure 1. Isolation, immortalization, and characterization of murine retinal, choroidal and brain endothelial cells**

(A) Workflow for generation of immortalized retinal endothelial cells (REC), choroidal endothelial cells (ChEC), and brain endothelial cells (BEC) from P30 and P15 mice (129/Sv), respectively. Endothelial cells (EC) were specifically immortalized by transducing primary cultures with the polyoma virus middle T antigen on days 1 and 2.

(B) Immunofluorescence staining of REC, ChEC, and BEC for platelet endothelial cell adhesion molecule 1 (PECAM1, green) on day 60 of culture. Cell nuclei were counter stained with DAPI (blue). Scale bar: 50 μm.

(C) Normalized counts for select endothelial (cluster of differentiation 34 [*Cd34*], cadherin 5 [*Cdh5*], claudin 5 [*Cldn5*], Fms related receptor tyrosine kinase 1 [*Flt1*], intercellular adhesion molecule 1 [*Icam1*, *Cd54*], kinase insert domain receptor [*Kdr*, *Vegfr2*], platelet and endothelial cell adhesion molecule 1 [*Pecam1*, *Cd31*] and TEK receptor tyrosine kinase [*Tek*, *Tie2*]) and non-endothelial stromal cell markers (α2-actin [*Acta2*], alanyl aminopeptidase, membrane [*Anpep*], chondroitin sulfate proteoglycan 4 [*Cspg4*], desmin [*Des*], platelet-derived growth factor receptor alpha [*Pdgfra*], platelet-derived growth factor receptor beta [*Pdgfrb*]) are shown.

*n* = 3. Data are represented as mean ± SEM.

cells (Table S1). These 21 genes included genes involved in endothelial proliferation (fatty acid binding protein 4 [*Fabp4*]) and the development of insulin resistance and atherosclerosis in relation to low-grade and chronic inflammation (*Fabp4*),[28,29] insulin growth factor (IGF) 2 signaling and regulation of glucose metabolism (*Igf2*)[30] and endothelial motility and proliferation (fibulin 5 [*Fbln5*]).[31] These differences were reflected in the principal-component analysis (PCA) that allowed a PCA-based differentiation of the cell lines (Figure 2B). Nevertheless, in comparison to the ChEC line, these differences were very minor (Figure 2B). Therefore, we grouped REC and BEC in the following and focused on their transcriptional changes in comparison to ChEC.

Nanopore RNA sequencing identified 493 differentially expressed genes between ChEC and REC/BEC (Figure 2A; Table S1). Differentially expressed genes between REC/BEC and ChEC were subjected to unsupervised hierarchical clustering resulting in four main clusters (Figure 2A). Clusters 1 (231 genes) and 2 (49 genes) represent weakly and strongly upregulated genes in ChEC, respectively, whereas clusters 3 (177 genes) and 4 (36 genes) contain weakly and strongly downregulated genes in ChEC, respectively. The clusters were analyzed by gene enrichment analyses to assign gene ontologies, potential affected signaling pathways, and to identify potential transcriptional regulators (Table 1).

Gene ontology enrichment of clusters 1 and 2 (= significantly upregulated genes in ChEC vs. REC/BEC) revealed, among the five top regulated hits, "positive regulation of epithelial to mesenchymal transition (EMT)" and "branching involved in blood vessel morphogenesis" (Table 1).

When analyzing potential pathways that might be affected by the significantly upregulated genes in clusters 1 and 2, we identified e.g., "HIF-1/2-alpha transcription factor network," "vascular endothelial growth factor receptor (VEGFR) 1 specific signals,"

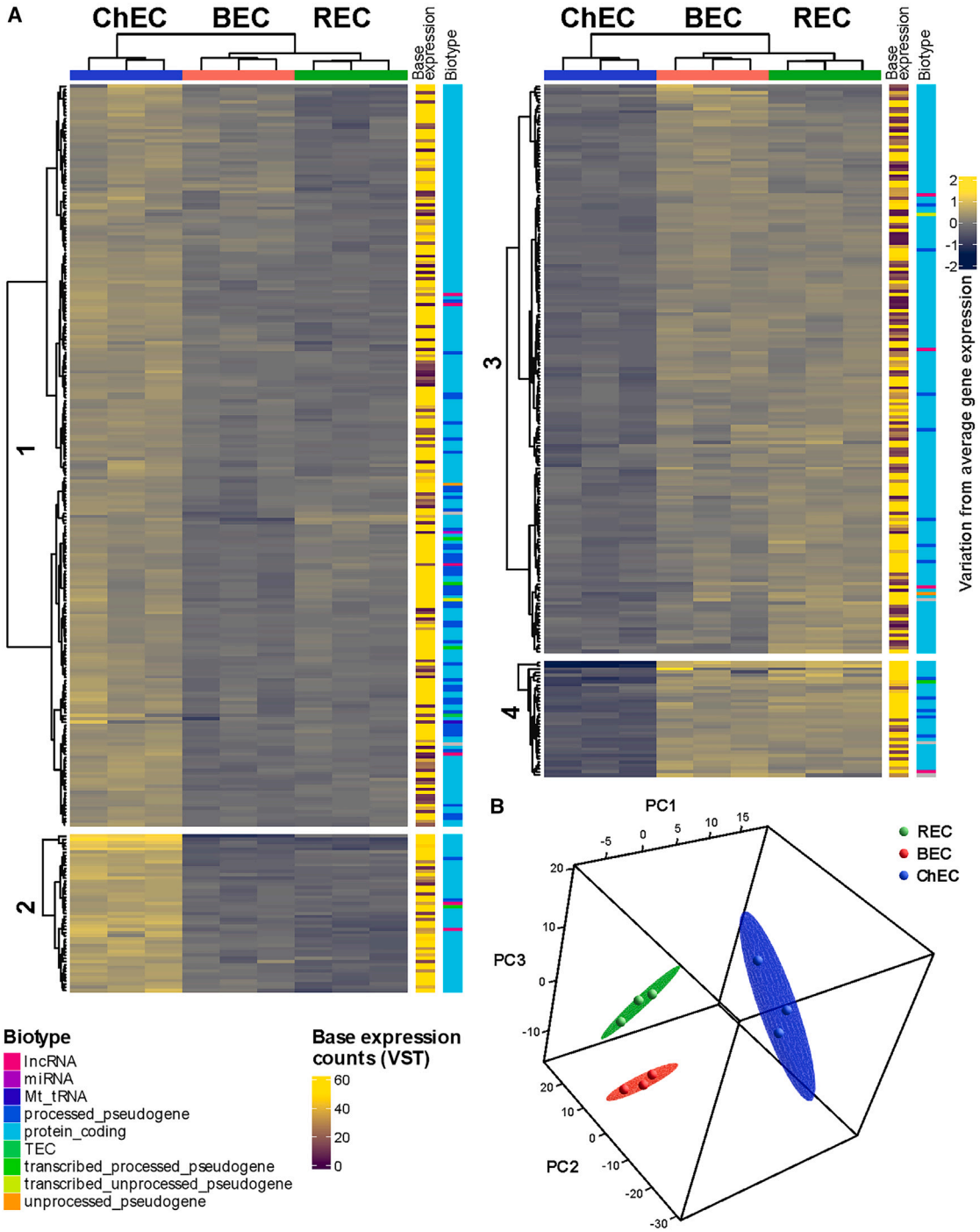


**Figure 2. Nanopore RNA sequencing analyses of immortalized endothelial cells**

Immortalized retinal endothelial cells (REC), choroidal endothelial cells (ChEC), and brain endothelial cells (BEC) were analyzed by long-range RNA sequencing ($n$ = 3 per cell line).

(A) Clustering analysis of significantly differentially expressed genes (DESeq2; BH $p$-adjusted <0.05) between any of the pairwise comparisons using VST-transformed normalized counts. Genes were grouped by unsupervised hierarchical clustering resulting in four main clusters and gene ontology enrichment was analyzed (Table 1).

(B) PCA analysis showed separate clustering of the samples per cell line indicating distinct transcriptomic regulation.

**Table 1. Enrichment analyses of the four clusters of differentially expressed genes between ChEC and REC/BEC**

| | Type | Database | Name | Combined score |
|---|---|---|---|---|
| Cluster 1 (231 genes) | Transcriptional regulation | ChEA 2022 | CEBPD, HIF1A, ESR1 | 38.20, 36.52, 31.50 |
| | | ENCODE TF ChIP-seq 2015 | NELFE, POLR2A, TAF7 | 60.63, 25.91, 23.32 |
| | Pathway | Reactome 2022 | Eukaryotic translation elongation | 369.81 |
| | | | Peptide chain elongation | 321.76 |
| | | | mRNA activation upon binding of cap-binding complex and eIFs, subsequent binding to 43S | 290.86 |
| | | | Nonsense mediated decay (NMD) independent of exon junction complex (EJC) | 226.62 |
| | | | Translation initiation complex formation | 219.07 |
| | | BioPlanet 2019 | Activation of mRNA upon binding of the cap-binding complex and eIFs, and subsequent binding to 43S | 397.40 |
| | | | Translation | 267.09 |
| | | | Cytoplasmic ribosomal proteins | 171.78 |
| | | | Influenza viral RNA transcription and replication | 168.61 |
| | | | Binding of RNA by insulin-like growth factor 2 mRNA binding proteins (IGF2BPs/IMPs/VICKZs) | 163.22 |
| | | NCI-Nature 2016 | HIF-1-alpha transcription factor network | 80.15 |
| | | | VEGFR1 specific signals | 61.24 |
| | | | Glypican 1 network | 61.24 |
| | | | Syndecan-4-mediated signaling events | 48.79 |
| | | | TGF-beta receptor signaling | 39.60 |
| | Gene ontology | GO Biological Process 2021 | Branching involved in blood vessel morphogenesis | 387.14 |
| | | | Regulation of inward rectifier potassium channel activity | 384.67 |
| | | | Positive regulation of CD4-positive, alpha-beta T cell proliferation | 384.67 |
| | | | Positive regulation of epithelial to mesenchymal transition involved in endocardial cushion formation | 384.67 |
| | | | Positive regulation of transcription from RNA polymerase II promoter in response to hypoxia | 384.67 |
| Cluster 2 (49 genes) | Transcriptional regulation | ChEA 2022 | CLOCK, NUCKS1, PPARG | 127.62, 90.66, 63.02 |
| | | ENCODE TF ChIP-seq 2015 | GABPA, GATA2, TCF12 | 59.76, 30.45, 20.68 |
| | Pathway | Reactome 2022 | Scavenging by class A receptors | 914.02 |
| | | | Binding and uptake of ligands by scavenger receptors | 608.21 |
| | | | PTK6 expression | 457.85 |
| | | | Arachidonate production from DAG | 457.85 |
| | | | MECP2 regulates transcription factors | 457.85 |
| | | BioPlanet 2019 | Platelet amyloid precursor protein pathway | 1444.55 |
| | | | Fibroblast growth factor 1 | 1175.54 |
| | | | Bone mineralization regulation | 759.09 |
| | | | Vitamin C in the brain | 759.09 |
| | | | Hormone-sensitive lipase (HSL)-mediated triacylglycerol hydrolysis | 667.81 |
| | | NCI-Nature 2016 | HIF-1-alpha transcription factor network | 307.83 |
| | | | Beta1 integrin cell surface interactions | 153.89 |
| | | | HIF-2-alpha transcription factor network | 152.68 |
| | | | Beta3 integrin cell surface interactions | 109.57 |
| | | | Beta5, beta6, beta7, and beta8 integrin cell surface interactions | 83.00 |

(*Continued on next page*)

**Table 1.** *Continued*

| | Type | Database | Name | Combined score |
|---|---|---|---|---|
| | Gene ontology | GO Biological Process 2021 | Regulation of vascular associated smooth muscle cell apoptotic process | 1529.01 |
| | | | Fructose 1,6-bisphosphate metabolic process | 1027.07 |
| | | | Negative regulation of bone mineralization | 533.96 |
| | | | Protein localization to cell surface | 522.20 |
| | | | Myoblast differentiation | 483.62 |
| Cluster 3 (177 genes) | Transcriptional regulation | ChEA 2022 | FOXP1, GATA2, KLF4 | 76.88, 40.21, 36.67 |
| | | ENCODE TF ChIP-seq 2015 | GABPA, EP300, HCFC1 | 13.87, 12.63, 10.87 |
| | Pathway | Reactome 2022 | Formyl peptide receptors bind formyl peptides and many other ligands | 232.64 |
| | | | Regulation of commissural axon pathfinding by SLIT and ROBO | 191.45 |
| | | | Type I hemidesmosome assembly | 191.45 |
| | | | Non-integrin membrane-ECM Interactions | 166.56 |
| | | | Pyrimidine salvage | 138.52 |
| | | BioPlanet 2019 | ADP signaling through P2Y purinoceptor 1 | 383.68 |
| | | | Formyl peptide interaction with formyl peptide receptors | 232.64 |
| | | | Pyrimidine salvage reactions | 191.45 |
| | | | Integrin beta-4 pathway | 138.52 |
| | | | Axonal growth stimulation | 88.27 |
| | | NCI-Nature 2016 | Alpha6 beta4 integrin-ligand interactions | 138.52 |
| | | | a6b1 and a6b4 integrin signaling | 81.60 |
| | | | Syndecan-3-mediated signaling events | 69.95 |
| | | | Signaling events mediated by PRL | 43.63 |
| | | | Rapid glucocorticoid signaling | 43.08 |
| | Gene ontology | GO Biological Process 2021 | Regulation of defense response to bacterium | 911.48 |
| | | | Positive regulation of defense response to bacterium | 232.64 |
| | | | Regulation of tumor necrosis factor superfamily cytokine production | 191.45 |
| | | | Mesodermal cell differentiation | 191.45 |
| | | | Gliogenesis | 189.51 |
| Cluster 4 (36 genes) | Transcriptional regulation | ChEA 2022 | SMAD1, STAT6, IKZF1 | 52.88, 52.74, 38.17 |
| | | ENCODE TF ChIP-seq 2015 | MEF2C, ZZZ3, STAT5A | 27.51, 16.25, 16.13 |
| | Pathway | Reactome 2022 | Chylomicron clearance | 696.01 |
| | | | Activation of RAC1 downstream of NMDARs | 431.21 |
| | | | Anchoring fibril formation | 431.21 |
| | | | CREB1 phosphorylation through activation of CaMKII/CaMKK/CaMKIV cascasde | 358.46 |
| | | | Activation of Ca-permeable kainate receptor | 305.06 |
| | | BioPlanet 2019 | Pertussis toxin-insensitive CCR5 signaling in macrophage | 582.78 |
| | | | ADP signaling through P2Y purinoceptor 1 | 535.47 |
| | | | G beta-gamma signaling through PI3K gamma | 535.47 |
| | | | Low-density lipoprotein (LDL) pathway during atherogenesis | 535.47 |
| | | | MSP/RON receptor signaling pathway | 535.47 |

(*Continued on next page*)

**Table 1.** *Continued*

| Type | Database | Name | Combined score |
|---|---|---|---|
| | NCI-Nature 2016 | Rapid glucocorticoid signaling | 358.46 |
| | | N-cadherin signaling events | 242.77 |
| | | PAR4-mediated thrombin signaling events | 153.07 |
| | | Regulation of cytoplasmic and nuclear SMAD2/3 signaling | 129.39 |
| | | Cellular roles of anthrax toxin | 111.44 |
| Gene ontology | GO Biological Process 2021 | Macrophage chemotaxis | 1033.62 |
| | | Macrophage migration | 752.09 |
| | | Negative regulation of cholesterol biosynthetic process | 696.01 |
| | | Negative regulation of cholesterol metabolic process | 696.01 |
| | | Negative regulation of insulin-like growth factor receptor signaling pathway | 696.01 |

Enriched pathways, gene ontologies, and transcriptional regulators were predicted using Enrichr. For pathways and gene ontologies only the top five, non-redundant hits are shown. For transcriptional regulators the top three, non-redundant hits are shown.

and "transforming growth factor (TGF)-β receptor signaling." We further visualized these signaling pathways (TGF-β signaling: Figure 3, HIF-1α signaling: Figure 4A, and VEGF signaling: Figure 4B) as heatmaps. Unsupervised hierarchical clustering of the individual pathways showed a clear separation between ChEC and REC/BEC for several of the associated genes. Furthermore, k-mer analysis (k-mer groups are indicated on the left side of each heatmap) showed clusters of tightly co-regulated genes.

Gene ontology analyses of cluster 3 and 4 (= significantly downregulated genes in ChEC vs. REC/BEC) indicated among others, "regulation of tumor necrosis factor superfamily cytokine production" and "macrophage chemotaxis/migration." Moreover, when studying potential pathways that might be affected by the significantly downregulated genes in cluster 3 and 4, we identified among others, "rapid glucocorticoid signaling," "alpha6 beta1/4 integrin signaling," "syndecan-3-mediated signaling events," and "regulation of cytoplasmic and nuclear SMAD2/3 signaling" (Table 1).

We also investigated whether a cell line-specific transcriptional profile exists that could provide clues to the changes occurring in the pathology of DR or AMD. Thus, we analyzed the alterations of "glucose transmembrane transport" as a potential indicator for a sensitivity of REC/BEC toward DR related alterations. Moreover, we studied "complement system" and "matrix degeneration" since these are processes associated with AMD and DR.[4,7,32] Again, we visualized these signaling pathways as heatmaps (glucose transmembrane transport: Figure S3, complement system: Figure S4A, matrix degeneration: Figure S4B). Clustering analysis (k-mer groups are shown on the left side of each heatmap) showed groups of tightly co-regulated genes and a clear separation between ChEC and REC/BEC for several genes.

Intriguingly, when studying "glucose transmembrane transport" genes such as alveolar soft part sarcoma chromosomal region candidate gene 1 protein (*Aspsrc1*) and protein kinase C alpha type (*Prkca)* were higher expressed in REC/BEC compared to ChEC (Figure S3). Moreover, in an AMD-related context, it is of interest to note that complement factor H (*Cfh*), which has an essential role in the regulation of complement activation was lower expressed in ChEC than in REC/BEC (Figure S4A).[33] Additionally, genes of the matrix metalloproteinase (MMP) family that are involved in the breakdown of extracellular matrix cluster were also differentially expressed, with e.g., MMP14 being higher expressed in ChEC than in REC/BEC (Figure S4B).

## Functional analyses regarding the barrier properties of REC, BEC, and ChEC

Next, we investigated barrier properties of confluent REC, BEC, and ChEC monolayers in functional permeability assays *in vitro*. Tight junctions between retinal endothelial cells form the inner BRB and between brain endothelial cells form the BBB, respectively, and the endothelium of the choriocapillaris is fenestrated.[1] Therefore, our expectation was to observe relatively low permeability of REC and BEC and relatively high permeability of ChEC. However, there was no difference in permeability for fluorescein (332 Da) between REC, BEC and ChEC monolayers (Figure 5C). As the cells had been removed from their physiological environment and had been immortalized, we hypothesized that barrier formation of REC, BEC, and/or fenestration of ChEC was lost or decreased *in vitro*. However, our transcriptomic data showed that well-known BBB/iBRB genes[3,34] were still detectable (70 genes), among them, 17 genes clustered as higher expressed in REC/BEC compared to ChEC (Figure S5). We also analyzed the expression of transporters in REC, BEC, and ChEC by using the gene lists of the gene ontology clusters "active transmembrane transporter activity (GO:0022804)" (Figure S6A) and "transport across blood brain barrier (GO:0150104)" (Figure S6B). Comparable to our analyses before, the main differences in the gene expression profile of these markers where evident between ChEC and REC/BEC. Expression of BBB/iBRB markers is regulated by the Wnt/β-catenin signaling pathway in CNS endothelial cells.[35,36] The Wnt agonists WNT7A and WNT7B expressed by astrocytes, oligodendrocytes and neurons in the brain and norrin, expressed by Müller cells in the retina instruct CNS endothelial cells to form the BBB/iBRB.[37,38] Hence, to reactivate Wnt/β-catenin signaling and barrier formation in REC and BEC, we stimulated them with the Wnt/β-catenin activator CHIR99021 (laduviglusib).[39]

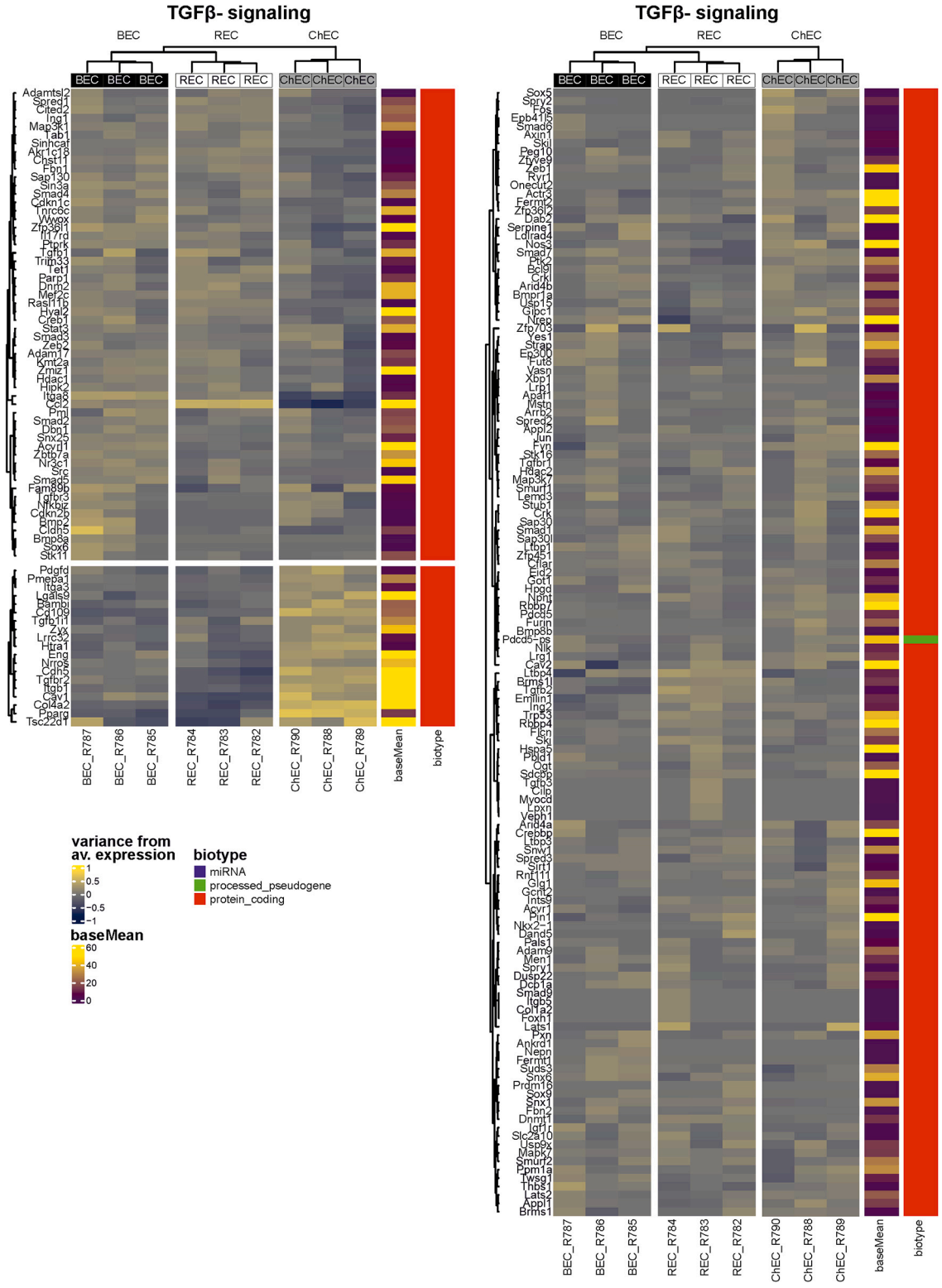


**Figure 3. Analysis of TGF-β signaling**

Genes associated with "cellular response to transforming growth factor β stimulus" (GO:0071560) were used to generate a VST-transformed expression matrix. This matrix was used for clustering analysis using ComplexHeatmap with a k of 3.

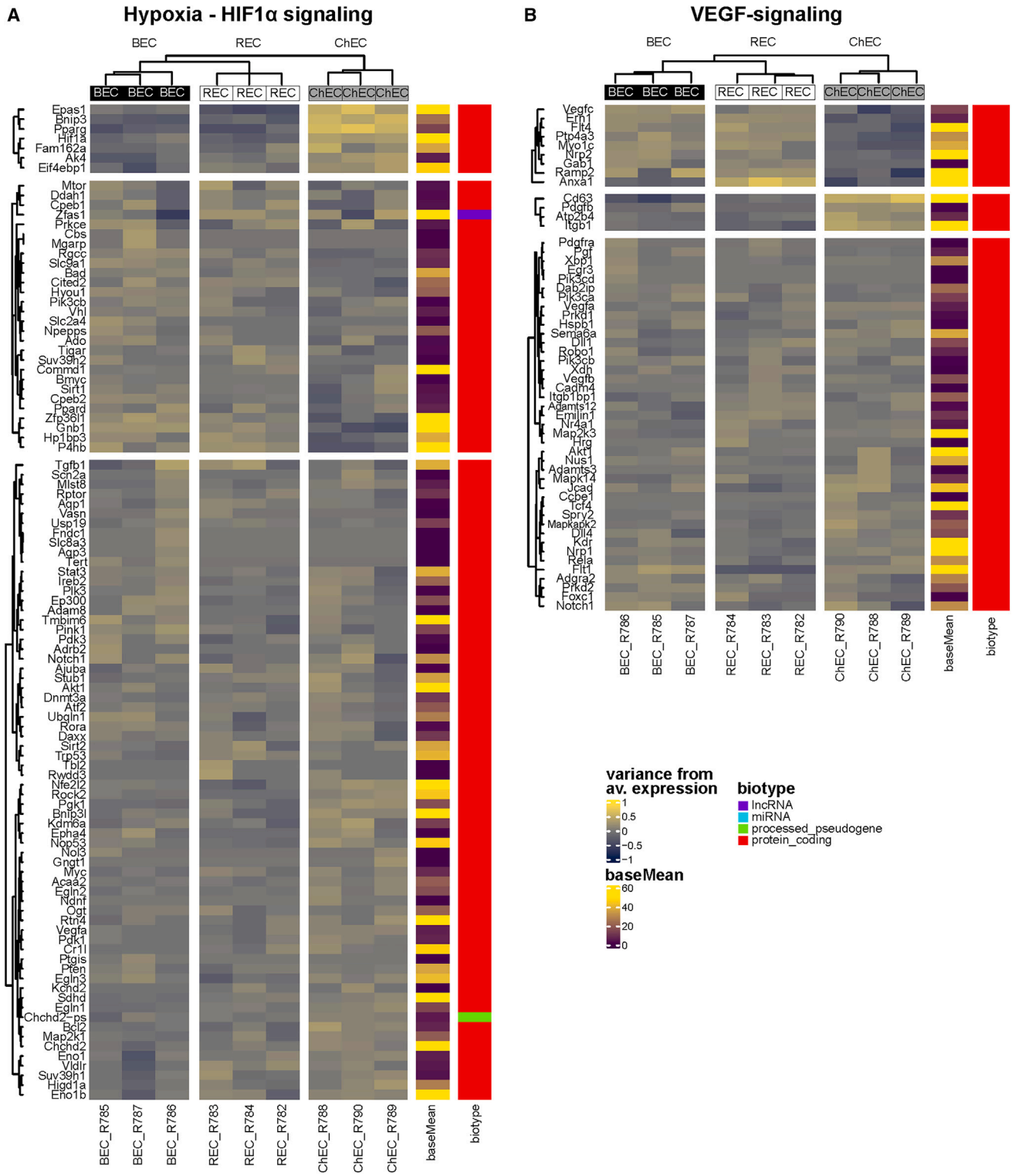


**Figure 4. Analysis of hypoxia/Hif1a- and VEGF signaling**

(A) Genes associated with "cellular response to hypoxia" (GO:0071456) were used to generate a VST-transformed expression matrix. This matrix was used for clustering analysis using ComplexHeatmap with a k of 3.

(B) Genes associated with "cellular response to vascular endothelial growth factor stimulus" (GO:0035924) were used to generate a VST-transformed expression matrix. This matrix was used for clustering analysis using ComplexHeatmap with a k of 3.

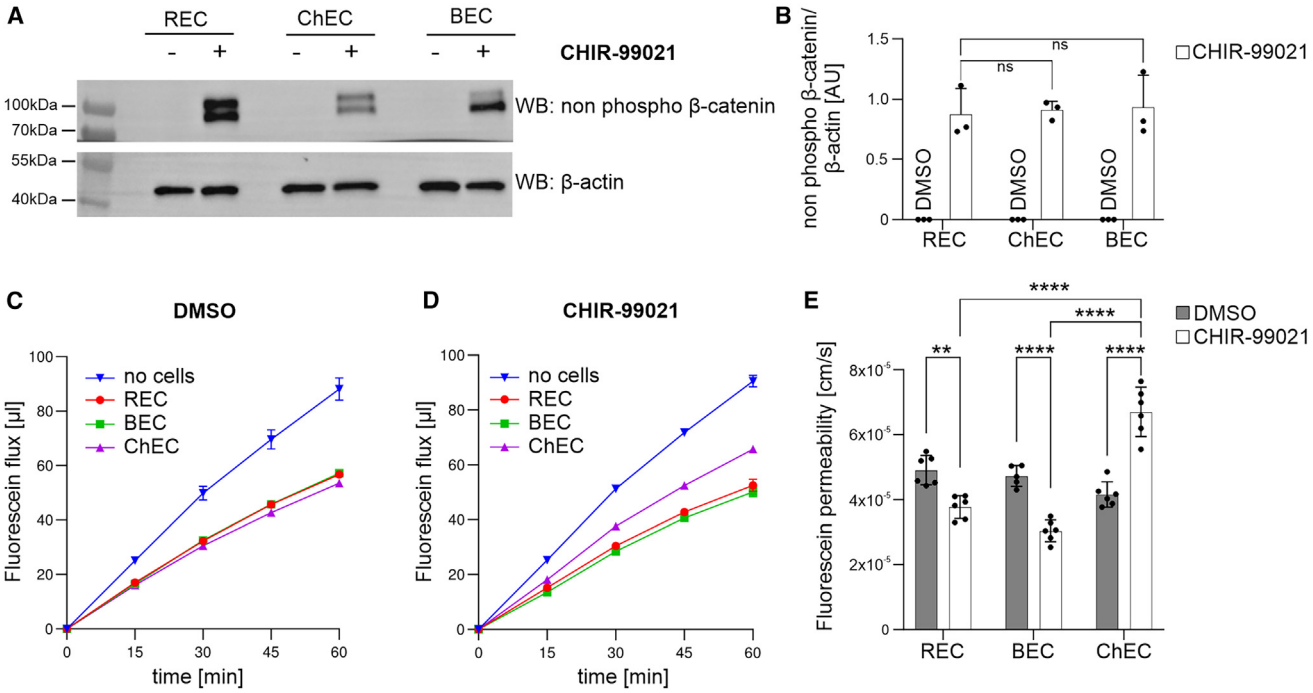


**Figure 5. WNT-pathway stimulation and permeability of REC, ChEC, and BEC monolayers for fluorescein**

(A) Representative western blots of non-phosphorylated (Ser45) β-catenin and β-actin of REC, ChEC and BEC incubated with medium containing 10μM CHIR99021 (+) or control medium (–).

(B) Densitometric evaluation of non-phosphorylated (Ser45) β-catenin western blot band intensity, normalized to β-actin band intensity. ($n$ = 3, data are represented as mean ± SD).

(C and D) Fluorescein flux over time through transwell filters only (no cells) or DMSO- (C) or CHIR99021-treated (10 μM for 7 days) (D) REC, ChEC, BEC monolayers ($n$ = 3, data are represented as mean ± SD).

(E) Fluorescein permeability coefficients calculated from the slopes in (A) and (B) ($n$ = 12, data are represented as mean ± SD, $^{**}p < 0.002$, $^{****}p < 0.0001$).

Indeed, CHIR99021 treatment resulted in stabilization of non-phosphorylated β-catenin compared to DMSO-treated controls (Figures 5A and 5B), thus confirming a robust activation of the Wnt/β-catenin signaling pathway. Moreover, as expected CHIR99021 treatment resulted in decreased permeability of REC and BEC (Figures 5D and 5E). Yet surprisingly, permeability of ChEC monolayers increased upon CHIR99021 stimulation (Figures 5D and 5E), indicating that Wnt/β-catenin stimulation affects barrier formation only in endothelial cells originating from the CNS. To further investigate whether this observation might be caused by e.g., an altered expression or localization of tight junction proteins such as CLDH5 and TJP1/ZO1 or PLVAP, we performed immunohistochemical staining and protein quantification. Intriguingly, CLDN5 (Figures S7A and S7B) of DMSO-treated compared to CHIR-99021 treated cells showed a decreased expression in REC and ChEC, but an increased expression in BEC. PLVAP expression significantly decreased in REC, ChEC and BEC following CHIR-99021 treatment (Figures S7C, S7D, S8A, and S8B). Here, it worthwhile to mention that the expression pattern of PLVAP changed from a more or less homogeneous and rather weak distribution in DMSO-treated REC, BEC, and ChEC to a punctiform and distinct localization only in CHIR-99021-treated ChEC cells (Figure S7C, insert). As expected upon WNT stimulation, expression of TJP1/ZO1 significantly increased in all three cell lines (Figures S7E and S7F).

## DISCUSSION

In this study, we describe a robust protocol to generate murine immortalized retinal, choroidal, and brain endothelial cell cultures. We generated in-depth transcriptomic datasets and discovered striking transcriptional similarities of retinal and brain endothelial cells but identified 493 differentially expressed genes between choroidal endothelial cells and retinal/brain endothelial cells. Subsequently performed gene ontology analyses indicated changes in the modulation of the immune system and dysregulation of pathways like HIF-1/2α-, TGF-β-, and VEGF signaling. Besides that, we discovered differences in the transcriptional profile of the cell lines, which indicate susceptibility of the respective endothelial cells, depending on their tissue origin, to pathophysiological changes occurring in DR and AMD. Moreover, we demonstrated that the cell lines retained barrier function *in vitro* and that activation of the Wnt/β-catenin signaling pathway restored BBB/iBRB properties in BEC and REC, but surprisingly increased permeability of ChEC.

The striking similarity between REC and BEC confirmed previous reports that endothelial cells constituting the inner BRB and BBB, respectively, are highly similar.[40] Whether the differentially expressed genes in REC vs. BEC represent subtle differences between the iBRB and BBB *in vivo* or arise from differences in the isolation and/or yield of primary cells from retina vs. brain

remains to be determined. The large differences of BEC/REC to ChEC might be due to the different types of endothelial cells that are generally categorized in continuous, fenestrated and discontinuous/sinusoidal, depending on their morphological appearance and their degree of permeability.[41] Accordingly, *in vivo*, choroidal endothelial cells are fenestrated and retinal/brain endothelial cells are continuous, forming even the inner BRB and BBB, through tight junctions, respectively.[1] However, immunohistochemical PLVAP staining and extraction of the normalized counts of *Plvap*, which is a marker for fenestrated endothelial cells,[27] showed no significant differences between the three cell lines indicating that this well-described phenotypic difference *in vivo* is not applicable in these immortalized cell lines *in vitro*. In fact, unlike primary endothelial cells or endothelial cells immortalized by other means (e.g., hCMEC/D3), our cells have been immortalized using the middle T antigen (mT) and grow completely independent of exogenously added growth factors. Intriguingly, the widely used murine brain endothelial cell line bEnd.3 was also immortalized using mT.[20] Besides being a potent oncogene, mT is a strong mitogene. It inhibits protein phosphatase 2A (PP2A) and activates Src family kinases, which in turn phosphorylate mT. Once phosphorylated, mT mimics a constitutively active receptor tyrosine kinase (RTK) activating SHC-transforming protein 1 (SHC1), 14-3-3 protein, phosphoinositide 3-kinase (PI3K), and phospholipase Cγ1 (PLCγ1) signaling pathways.[42] Thus, the equalization of PLVAP levels in the three cell lines might well be a result of to the robust activation of RTK and/or *ex vivo* cell culture conditions.

When analyzing potential pathways that might be affected by the significantly upregulated genes in ChEC compared to REC/BEC (clusters 1 and 2), we identified e.g., HIF-1/2α-, VEGF-, and TGF-β signaling. All of these signaling pathways critically contribute to the finely orchestrated interplay during angiogenesis and in maintaining the mature vasculature.[8,11,43–46] Besides that, TGF-β signaling also plays a pivotal role in EMT and endothelial-mesenchymal transition (EndMT).[47] Intriguingly, gene ontology (GO) analyses of the transcriptomic signature of ChEC also indicated differences in epithelial to mesenchymal transition (EMT) and vessel morphogenesis. EMT describes a biologic process by which epithelial cells become cells with a mesenchymal phenotype.[48] Accordingly, EndMT describes the transition of endothelial cells toward a mesenchymal phenotype and is considered a subcategory of EMT.[49] Intriguingly, in late stages of AMD, both, EMT and EndMT critically contribute to the pathogenesis of subretinal fibrosis.[49] Thus, based on the transcriptomic profile of ChEC, it is tempting to speculate that these cells are more likely to undergo EMT/EndMT than retinal/brain endothelial cells, and thus contribute to the described phenotypic alterations in AMD. Accordingly, based on the transcriptomic signatures of REC/BEC and/or ChEC, an imbalance in HIF-1/2α-, VEGF-, and TGF-β signaling pathways may drive the molecular pathogenesis of DR or neovascular AMD, respectively.[4,5]

Intriguingly, gene ontology analyses of the downregulated genes in ChEC (compared to REC/BEC) identified groups of genes with attributed function in regulation of "tumor necrosis factor superfamily cytokine production" and "macrophage chemotaxis/migration." Tumor necrosis factor (TNF) cytokines are involved in regulating endothelial barrier properties and in microglia/macrophage reactivity.[50,51] We also identified "rapid glucocorticoid signaling" and "syndecan-3-mediated signaling events" as downregulated pathways in ChEC versus REC/BEC. Recent data demonstrate that (endogenous) glucocorticoids, acting through the glucocorticoid receptor on endothelial cells, negatively regulate inflammation.[52] Syndecan-3 is a member of the multifunctional family of cell surface molecules and current studies suggest involvement in inflammatory disorders and angiogenesis.[53] Hence, this finding might indicate that the transcriptional profile of choroidal endothelial cells, when translated to the protein level, contribute to a quiescent, immune-modulating environment. We also identified "alpha6 beta1/4 integrin signaling," and "regulation of cytoplasmic and nuclear SMAD2/3 signaling" as downregulated pathways in ChEC versus REC/BEC. Integrin α6β1 and α6β4 are laminin-binding receptors and expressed on endothelial cells.[54] The role of α6β4 integrin in angiogenesis, vessel maturation and stability, is controversially discussed as depending on the experimental settings, pro- and anti-angiogenic properties have been reported.[55–58] Integrin α6β1 is reported to promote tumor angiogenesis, invasiveness, and cancer progression.[59] SMAD2/3 are components of the canonical TGF-β signaling pathway.[60] Accordingly, our group recently showed that deletion of the TGF-β signaling pathway resulted in microaneurysms of the intraretinal vessels and choroidal neovascularization as observed in humans suffering from DR or nAMD, respectively, indicating that TGF-β signaling is essential for stabilization and maintenance of the vasculature.[8,11]

We furthermore identified cell line-specific transcriptional profiles with alterations in glucose transmembrane transport, complement-signaling and ECM-degeneration that might sensitize the specific endothelial cells to alterations occurring in DR or AMD. Clearly, endothelial dysfunction in DR is a multifactorial driven process through e.g., accumulating advanced glycosylation end products (AGEs) and receptors (RAGE), disruption of peroxisome proliferator-activated receptor-γ (PPARγ), oxidative stress, leukostasis, chronic inflammation, and altered expression levels of cytokines, growth factors such as VEGF, and microRNA (miRNA) networks.[5,7,61–65] However, in the glucose transmembrane transport analyses, among others, genes such as *Aspsrc1* and *Prkca* were among the higher expressed genes in REC/BEC compared to ChEC. In this context, *Aspsrc1* is described to modulate the amount of GLUT4 that is available at the cell surface[66] and *Prkca* is involved in the stabilization of *Vegfa* mRNA at the post-transcriptional level and mediates VEGFA-induced cell proliferation.[67] Yet, to our understanding it is well thinkable that the individual transcriptional profile of retinal endothelial cells sensitizes them to pathological alterations occurring in e.g., DR.

AMD is a multifactorial disease with the RPE and the choriocapillaris as central points of AMD pathogenesis.[4,68–71] Yet, in late stage nAMD, proliferation of choroidal endothelial cells results in the formation of choroidal neovascularization, which is a key process in nAMD pathogenesis.[4] In addition to endothelial proliferation, changes in the local microenvironment are essential to allow CNV penetration through the extracellular matrix structure of the Bruch's membrane and the tight junctions of the RPE.

Hence, it is possible that besides endothelial proliferation, choroidal endothelial cells also contribute to AMD pathogenesis through generation of a specific microenvironment that promotes matrix degeneration and a higher susceptibility toward alterations of the complement system. Based on their individual transcriptional profile it is likely that the cells are sensitized toward pathological alterations occurring in nAMD.

Immortalization alters endothelial cell biology to a certain extent, and culturing endothelial cells as monocultures results in further changes, even in primary endothelial cells. Primary brain endothelial cells, for example, loose BBB properties and expression of BBB markers within a few days in culture.[72] Tissue-specific properties of the endothelium are usually induced and maintained by paracrine factors from parenchymal cells. *In vivo* BBB marker expression in brain endothelium is induced by activation of the Wnt/β-catenin signaling pathway by the glia-derived factors WNT7A/7B and norrin.[35,38] Co-culturing brain endothelial cells with astrocytes or pericytes or stimulating them with the Wnt/β-catenin signaling activator CHIR99021 (laduviglusib) leads to re-expression of BBB markers and increased barrier properties *in vitro.*[39,72,73] Conversely, permeability and fenestrations in choriocapillaris endothelium are induced by RPE-derived vascular endothelial growth factor (VEGF).[74,75] Since our *in vitro* permeability assays using REC, ChEC, and BEC monolayers showed no differences in permeability for fluorescein, we used CHIR-99021 to potentially restore iBRB properties in REC/BEC.[39] Indeed, permeability of REC/BEC monolayers for fluorescein decreased upon CHIR-99021 treatment. Unexpectedly, CHIR-99021 treatment had the opposing effect on ChEC monolayers by increasing their permeability for fluorescein. This was surprising as so far, Wnt/β-catenin signaling has not been implicated e.g., in fenestration formation in the endothelium of the choriocapillaris. In this context, it is worthwhile to mention that the staining pattern of PLVAP, a well-known structural protein of fenestrae, changed toward a punctuated and very distinct pattern only in CHIR-99021 stimulated ChEC. Based on this observation, it is tempting to speculate that upon Wnt-stimulation ChEC cells regain their fenestrae-forming properties. Moreover, Wang et al. demonstrated in an methchemical approach that β-catenin stabilization in endothelial cells *in vivo* resulted in a phenotypic conversion of endothelial cells of the choriocapillaris from their CLDN5-/PLVAP+ state to a CLDN5+/PLVAP− state,[76] an endothelial phenotype that resembles retinal/brain endothelial cells (CLDN5+/PLVAP−) and therefore would imply a reduced permeability. However, there are some reports indicating that in contrast to the rather robust barrier-restoring effect of Wnt activation in CNS-derived endothelial cells,[77–79] ectopic activation of Wnt signaling in peripheral (liver- and lung-derived) endothelial cells had only very minor effects e.g., on the expression of BBB genes.[80] In summary, Wnt activation impacts endothelial cells in a context dependent manner. To further elucidate the effect of Wnt signaling on choroidal endothelial cells, we plan to investigate this interplay in future studies.

## Conclusion

In summary, the protocol we describe here can be used to establish retinal and choroidal endothelial cell cultures from virtually any mouse line, and therefore can be used to study e.g., endothelial pathomechanisms of DR and AMD *in vitro*. Moreover, the cells might represent new experimental tools to screen for new therapeutic options. We furthermore showed that the cultured cells retained expression of certain barrier genes and that activation of the Wnt/β-catenin signaling pathway restored BBB/iBRB barrier function in retinal and brain endothelial cells, but increased permeability of choroidal endothelial cells. Nanopore RNA sequencing analyses of retinal, choroidal, and brain endothelial cells showed high transcriptional similarities between retinal and brain endothelial cells, but hundreds of differentially expressed genes in comparison to choroidal endothelial cells. The predominant transcriptional alterations point toward differences, depending on the tissue origin of the endothelial cells, in modulation of the immune system and dysregulation of pathways like HIF 1/2α-, TGF-β- and VEGF signaling. Thus, our findings highlight the centrality of these signaling pathways and of the ocular immune system in the pathogenesis of ocular diseases associated with endothelial proliferation such as DR and AMD.

## Limitations of the study

Mice of both sexes had been used to isolate the specific endothelial cells. In culture, the cells were not subjected to clonal selection. Therefore, the immortalized cells cannot be assigned to a specific sex. As briefly outline before, the endothelial cells have been immortalized using the middle T antigen (mT) that is not only a potent oncogene but also a strong mitogene. Consequently, activated (phosphorylated) mT mimics a constitutively active receptor tyrosine kinase (RTK) that activates SHC-transforming protein 1 (SHC1), 14-3-3 protein, phosphoinositide 3-kinase (PI3K), and phospholipase Cγ1 (PLCγ1) signaling pathways.[42] Consequently, this results in a permanent growth stimulus. Moreover, to generate endothelial monocultures the cells have been removed from their physiological microenvironment, which in addition to their immortalization, also might alter endothelial cell biology to a certain extent, even in primary endothelial cells.[72]

## RESOURCE AVAILABILITY

### Lead contact

Further information and requests for resources and reagents should be directed to and will be fulfilled by the lead contact Barbara M. Braunger (b.braunger@uke.de).

### Materials availability

This study did not generate new unique reagents. Chemical substances, animals, evaluation software and disposable materials are commercially available. The immortalized endothelial cell lines are available upon request from the lead contact.

### Data and code availability

- The raw nanopore RNA sequencing data are available, have been deposited in GEO and are publicly available at the date of publication. Accession number is listed in the key resources table.
- Software and employed codes are free or commercially available and listed in the STAR Methods section and the key resources table.
- Any additional information required to reanalyze the data reported in this paper is available from the lead contact upon request.

## ACKNOWLEDGMENTS

The authors wish to extend special thanks to Dr. D.A. Antonetti, Department of Ophthalmology and Visual Sciences, Kellogg Eye Center, University of Michigan, Ann Arbor, MI 48105, USA, Dr. N. Hudson and Dr. M. Campbell, Trinity College Dublin, Smurfit Institute of Genetics, Dublin, Ireland for inspiring and helpful discussions and suggestions. The authors furthermore thank Lucas Guizetti for illustrating the schematics in Figure 1 and the graphical abstract and we thank Alla Ganscher, Elke Stauber, and Elke Varin for the great technical assistance.

Funding: This work was supported by DFG grants Fo 315/5-1 (C.Y.F.), BR 4957/3-1 (B.M.B.), BR 4957/4-1 (B.M.B.), NE 2372/1-1 (A.N.) and DFG grant 440925599 (M.V.), the Jackstädt Foundation (B.M.B.) and the Helmut Ecker Foundation (B.M.B). The funders had no role in study design, data collection and analysis, decision to publish, or preparation of the manuscript.

## AUTHOR CONTRIBUTIONS

R.H.: data curation, formal analysis, investigation, methodology, writing – review & editing. L.H.: data curation, formal analysis, investigation, methodology, writing – original draft, writing – review & editing. J.S.B.: data curation, formal analysis, investigation, methodology, writing – original draft, writing – review & editing. M.V.: data curation, validation, methodology, writing – review & editing. A.S.: data curation, formal analysis, investigation, methodology, writing – review & editing. N.H.: data curation, formal analysis, investigation, methodology, writing – review & editing. S.E.: resources, supervision, writing – review & editing. F.H.: data curation, formal analysis, investigation, methodology, software, writing – original draft, writing – review & editing. M.W.: data curation, formal analysis, investigation, methodology, software, writing – original draft, writing – review & editing. A.N.: conceptualization, data curation, formal analysis, investigation, methodology, software, writing – original draft, writing – review & editing. C.Y.F.: conceptualization, project administration, supervision, data curation, resources, formal analysis, investigation, methodology, funding acquisition, writing – original draft, writing – review & editing. B.M.B.: conceptualization, project administration, supervision, data curation, resources, formal analysis, investigation, methodology, funding acquisition, writing – original draft, writing – review & editing. All authors read and approved the final manuscript.

## DECLARATION OF INTERESTS

The authors declare no competing interests.

## STAR★METHODS

Detailed methods are provided in the online version of this paper and include the following:

- KEY RESOURCES TABLE
- EXPERIMENTAL MODEL AND STUDY PARTICIPANT DETAILS
  - Mice
  - Immortalization and endothelial cell culture
  - Ethics approval and consent to participate
- METHOD DETAILS
  - Immunofluorescence staining
  - Third generation long-range RNA sequencing (nanopore)
  - Bioinformatics
  - Western Blot of active β-catenin and PLVAP
  - Permeability assay
- QUANTIFICATION AND STATISTICAL ANALYSIS

## SUPPLEMENTAL INFORMATION

Supplemental information can be found online at https://doi.org/10.1016/j.isci.2024.111740.

Received: March 7, 2024
Revised: July 9, 2024
Accepted: December 31, 2024
Published: January 2, 2025

## REFERENCES

1. Braunger, B.M., Gießl, A., and Schlötzer-Schrehardt, U. (2023). The Blood-ocular Barriers and their Dysfunction: Anatomy, Physiology, Pathology. Klin. Monbl. Augenheilkd. *240*, 650–661.
2. Cunha-Vaz, J., Bernardes, R., and Lobo, C. (2011). Blood-retinal barrier. Eur. J. Ophthalmol. *21*, S3–S9.
3. Daneman, R. (2012). The blood-brain barrier in health and disease. Ann. Neurol. *72*, 648–672.
4. Ambati, J., and Fowler, B.J. (2012). Mechanisms of age-related macular degeneration. Neuron *75*, 26–39.
5. Antonetti, D.A., Klein, R., and Gardner, T.W. (2012). Diabetic retinopathy. N. Engl. J. Med. *366*, 1227–1239.
6. Cheung, N., Mitchell, P., and Wong, T.Y. (2010). Diabetic retinopathy. Lancet *376*, 124–136.
7. Shityakov, S., Nagai, M., Ergun, S., Braunger, B.M., and Forster, C.Y. (2022). The Protective Effects of Neurotrophins and MicroRNA in Diabetic Retinopathy, Nephropathy and Heart Failure via Regulating Endothelial Function. Biomolecules *12*, 1113.
8. Braunger, B.M., Leimbeck, S.V., Schlecht, A., Volz, C., Jägle, H., and Tamm, E.R. (2015). Deletion of ocular transforming growth factor beta signaling mimics essential characteristics of diabetic retinopathy. Am. J. Pathol. *185*, 1749–1768.
9. Olivares, A.M., Althoff, K., Chen, G.F., Wu, S., Morrisson, M.A., DeAngelis, M.M., and Haider, N. (2017). Animal Models of Diabetic Retinopathy. Curr. Diab. Rep. *17*, 93.
10. Pennesi, M.E., Neuringer, M., and Courtney, R.J. (2012). Animal models of age related macular degeneration. Mol. Aspects Med. *33*, 487–509.
11. Schlecht, A., Leimbeck, S.V., Jägle, H., Feuchtinger, A., Tamm, E.R., and Braunger, B.M. (2017). Deletion of Endothelial Transforming Growth Factor-beta Signaling Leads to Choroidal Neovascularization. Am. J. Pathol. *187*, 2570–2589.
12. Bowman, P.D., Betz, A.L., and Goldstein, G.W. (1982). Primary culture of microvascular endothelial cells from bovine retina: selective growth using fibronectin coated substrate and plasma derived serum. In Vitro *18*, 626–632.
13. Grant, M.B., and Guay, C. (1991). Plasminogen activator production by human retinal endothelial cells of nondiabetic and diabetic origin. Invest. Ophthalmol. Vis. Sci. *32*, 53–64.
14. Keithahn, M.A., Aotaki-Keen, A.E., Schneeberger, S.A., Hjelmeland, L.M., and Morse, L.S. (1997). Expression of fibroblast growth factor-5 by bovine choroidal endothelial cells in vitro. Invest. Ophthalmol. Vis. Sci. *38*, 2073–2080.
15. Lopez-Quintero, S.V., Ji, X.Y., Antonetti, D.A., and Tarbell, J.M. (2011). A three-pore model describes transport properties of bovine retinal endothelial cells in normal and elevated glucose. Invest. Ophthalmol. Vis. Sci. *52*, 1171–1180.
16. Sakamoto, T., Sakamoto, H., Hinton, D.R., Spee, C., Ishibashi, T., and Ryan, S.J. (1995). In vitro studies of human choroidal endothelial cells. Curr. Eye Res. *14*, 621–627.
17. Adamson, R.H., Curry, F.E., Adamson, G., Liu, B., Jiang, Y., Aktories, K., Barth, H., Daigeler, A., Golenhofen, N., Ness, W., and Drenckhahn, D. (2002). Rho and rho kinase modulation of barrier properties: cultured endothelial cells and intact microvessels of rats and mice. J. Physiol. *539*, 295–308.
18. Forster, C., Silwedel, C., Golenhofen, N., Burek, M., Kietz, S., Mankertz, J., and Drenckhahn, D. (2005). Occludin as direct target for glucocorticoid-induced improvement of blood-brain barrier properties in a murine in vitro system. J. Physiol. *565*, 475–486.

19. Golenhofen, N., Ness, W., Koob, R., Htun, P., Schaper, W., and Drenckhahn, D. (1998). Ischemia-induced phosphorylation and translocation of stress protein alpha B-crystallin to Z lines of myocardium. Am. J. Physiol. *274*, H1457–H1464.

20. Montesano, R., Pepper, M.S., Möhle-Steinlein, U., Risau, W., Wagner, E.F., and Orci, L. (1990). Increased proteolytic activity is responsible for the aberrant morphogenetic behavior of endothelial cells expressing the middle T oncogene. Cell *62*, 435–445.

21. Blecharz, K.G., Drenckhahn, D., and Förster, C.Y. (2008). Glucocorticoids increase VE-cadherin expression and cause cytoskeletal rearrangements in murine brain endothelial cEND cells. J. Cereb. Blood Flow Metab. *28*, 1139–1149.

22. Forster, C., Waschke, J., Burek, M., Leers, J., and Drenckhahn, D. (2006). Glucocorticoid effects on mouse microvascular endothelial barrier permeability are brain specific. J Physiol *573*, 413–425.

23. Ittner, C., Burek, M., Störk, S., Nagai, M., and Förster, C.Y. (2020). Increased Catecholamine Levels and Inflammatory Mediators Alter Barrier Properties of Brain Microvascular Endothelial Cells in vitro. Front. Cardiovasc. Med. *7*, 73.

24. Williams, R.L., Courtneidge, S.A., and Wagner, E.F. (1988). Embryonic lethalities and endothelial tumors in chimeric mice expressing polyoma virus middle T oncogene. Cell *52*, 121–131.

25. Greene, C., Hanley, N., and Campbell, M. (2019). Claudin-5: gatekeeper of neurological function. Fluids Barriers CNS *16*, 3.

26. Herrnberger, L., Ebner, K., Junglas, B., and Tamm, E.R. (2012). The role of plasmalemma vesicle-associated protein (PLVAP) in endothelial cells of Schlemm's canal and ocular capillaries. Exp. Eye Res. *105*, 27–33.

27. Stan, R.V., Tkachenko, E., and Niesman, I.R. (2004). PV1 is a key structural component for the formation of the stomatal and fenestral diaphragms. Mol. Biol. Cell *15*, 3615–3630.

28. Elmasri, H., Karaaslan, C., Teper, Y., Ghelfi, E., Weng, M., Ince, T.A., Kozakewich, H., Bischoff, J., and Cataltepe, S. (2009). Fatty acid binding protein 4 is a target of VEGF and a regulator of cell proliferation in endothelial cells. FASEB J. *23*, 3865–3873.

29. Furuhashi, M. (2019). Fatty Acid-Binding Protein 4 in Cardiovascular and Metabolic Diseases. J. Atheroscler. Thromb. *26*, 216–232.

30. Holly, J.M.P., Biernacka, K., and Perks, C.M. (2019). The Neglected Insulin: IGF-II, a Metabolic Regulator with Implications for Diabetes, Obesity, and Cancer. Cells *8*, 1207.

31. Guadall, A., Orriols, M., Rodriguez-Calvo, R., Calvayrac, O., Crespo, J., Aledo, R., Martinez-Gonzalez, J., and Rodriguez, C. (2011). Fibulin-5 is up-regulated by hypoxia in endothelial cells through a hypoxia-inducible factor-1 (HIF-1alpha)-dependent mechanism. J. Biol. Chem. *286*, 7093–7103.

32. Nozaki, M., Raisler, B.J., Sakurai, E., Sarma, J.V., Barnum, S.R., Lambris, J.D., Chen, Y., Zhang, K., Ambati, B.K., Baffi, J.Z., and Ambati, J. (2006). Drusen complement components C3a and C5a promote choroidal neovascularization. Proc. Natl. Acad. Sci. USA *103*, 2328–2333.

33. Ferreira, V.P., Pangburn, M.K., and Cortés, C. (2010). Complement control protein factor H: the good, the bad, and the inadequate. Mol. Immunol. *47*, 2187–2197.

34. Franzen, O., Gan, L.M., and Bjorkegren, J.L.M. (2019). PanglaoDB: a web server for exploration of mouse and human single-cell RNA sequencing data. Database *2019*, baz046.

35. Stenman, J.M., Rajagopal, J., Carroll, T.J., Ishibashi, M., McMahon, J., and McMahon, A.P. (2008). Canonical Wnt signaling regulates organ-specific assembly and differentiation of CNS vasculature. Science *322*, 1247–1250.

36. Tran, K.A., Zhang, X., Predescu, D., Huang, X., Machado, R.F., Göthert, J.R., Malik, A.B., Valyi-Nagy, T., and Zhao, Y.Y. (2016). Endothelial beta-Catenin Signaling Is Required for Maintaining Adult Blood-Brain Barrier Integrity and Central Nervous System Homeostasis. Circulation *133*, 177–186.

37. Guerit, S., Fidan, E., Macas, J., Czupalla, C.J., Figueiredo, R., Vijikumar, A., Yalcin, B.H., Thom, S., Winter, P., Gerhardt, H., et al. (2021). Astrocyte-derived Wnt growth factors are required for endothelial blood-brain barrier maintenance. Prog Neurobiol *199*, 101937.

38. Wang, Y., Cho, C., Williams, J., Smallwood, P.M., Zhang, C., Junge, H.J., and Nathans, J. (2018). Interplay of the Norrin and Wnt7a/Wnt7b signaling systems in blood-brain barrier and blood-retina barrier development and maintenance. Proc. Natl. Acad. Sci. USA *115*, E11827–E11836.

39. Gastfriend, B.D., Nishihara, H., Canfield, S.G., Foreman, K.L., Engelhardt, B., Palecek, S.P., and Shusta, E.V. (2021). Wnt signaling mediates acquisition of blood-brain barrier properties in naive endothelium derived from human pluripotent stem cells. Elife *10*, e70992.

40. Li, Y., Faiz, A., Moshage, H., Schubert, R., Schilling, L., and Kamps, J.A. (2021). Comparative transcriptome analysis of inner blood-retinal barrier and blood-brain barrier in rats. Sci. Rep. *11*, 12151.

41. Hallmann, R., Horn, N., Selg, M., Wendler, O., Pausch, F., and Sorokin, L.M. (2005). Expression and function of laminins in the embryonic and mature vasculature. Physiol. Rev. *85*, 979–1000.

42. Fluck, M.M., and Schaffhausen, B.S. (2009). Lessons in signaling and tumorigenesis from polyomavirus middle T antigen. Microbiol. Mol. Biol. Rev. *73*, 542–563.

43. Apte, R.S., Chen, D.S., and Ferrara, N. (2019). VEGF in Signaling and Disease: Beyond Discovery and Development. Cell *176*, 1248–1264.

44. Carmeliet, P. (2003). Angiogenesis in health and disease. Nat. Med. *9*, 653–660.

45. Hashimoto, T., and Shibasaki, F. (2015). Hypoxia-inducible factor as an angiogenic master switch. Front. Pediatr. *3*, 33.

46. Walshe, T.E., Saint-Geniez, M., Maharaj, A.S.R., Sekiyama, E., Maldonado, A.E., and D'Amore, P.A. (2009). TGF-beta is required for vascular barrier function, endothelial survival and homeostasis of the adult microvasculature. PLoS One *4*, e5149.

47. Saito, A. (2013). EMT and EndMT: regulated in similar ways? J. Biochem. *153*, 493–495.

48. Kalluri, R., and Weinberg, R.A. (2009). The basics of epithelial-mesenchymal transition. J. Clin. Invest. *119*, 1420–1428.

49. Shu, D.Y., Butcher, E., and Saint-Geniez, M. (2020). EMT and EndMT: Emerging Roles in Age-Related Macular Degeneration. Int. J. Mol. Sci. *21*, 4271.

50. Marcos-Ramiro, B., García-Weber, D., and Millán, J. (2014). TNF-induced endothelial barrier disruption: beyond actin and Rho. Thromb. Haemost. *112*, 1088–1102.

51. Raffaele, S., Lombardi, M., Verderio, C., and Fumagalli, M. (2020). TNF Production and Release from Microglia via Extracellular Vesicles: Impact on Brain Functions. Cells *9*, 2145.

52. Zhou, H., Mehta, S., Srivastava, S.P., Grabinska, K., Zhang, X., Wong, C., Hedayat, A., Perrotta, P., Fernández-Hernando, C., Sessa, W.C., and Goodwin, J.E. (2020). Endothelial cell-glucocorticoid receptor interactions and regulation of Wnt signaling. JCI Insight *5*, e131384.

53. Arokiasamy, S., Balderstone, M.J.M., De Rossi, G., and Whiteford, J.R. (2019). Syndecan-3 in Inflammation and Angiogenesis. Front. Immunol. *10*, 3031.

54. Bouvard, C., De Arcangelis, A., Dizier, B., Galy-Fauroux, I., Fischer, A.M., Georges-Labouesse, E., and Helley, D. (2012). Tie2-dependent knockout of alpha6 integrin subunit in mice reduces post-ischaemic angiogenesis. Cardiovasc. Res. *95*, 39–47.

55. Desai, D., Singh, P., Van De Water, L., and Laflamme, S.E. (2013). Dynamic Regulation of Integrin alpha(6)beta(4) During Angiogenesis: Potential Implications for Pathogenic Wound Healing. Adv. Wound Care *2*, 401–409.

56. Nikolopoulos, S.N., Blaikie, P., Yoshioka, T., Guo, W., and Giancotti, F.G. (2004). Integrin beta4 signaling promotes tumor angiogenesis. Cancer Cell *6*, 471–483.

57. Welser, J.V., Halder, S.K., Kant, R., Boroujerdi, A., and Milner, R. (2017). Endothelial alpha6beta4 integrin protects during experimental autoimmune encephalomyelitis-induced neuroinflammation by maintaining vascular integrity and tight junction protein expression. J. Neuroinflammation *14*, 217.

58. Xu, H., and LaFlamme, S.E. (2022). Contribution of Endothelial Laminin-Binding Integrins to Cellular Processes Associated with Angiogenesis. Cells *11*, 816.

59. Mammadova-Bach, E., Zigrino, P., Brucker, C., Bourdon, C., Freund, M., De Arcangelis, A., Abrams, S.I., Orend, G., Gachet, C., and Mangin, P.H. (2016). Platelet integrin alpha6beta1 controls lung metastasis through direct binding to cancer cell-derived ADAM9. JCI Insight *1*, e88245.

60. Massague, J. (2000). How cells read TGF-beta signals. Nat. Rev. Mol. Cell Biol. *1*, 169–178.

61. Miyamoto, K., Hiroshiba, N., Tsujikawa, A., and Ogura, Y. (1998). In vivo demonstration of increased leukocyte entrapment in retinal microcirculation of diabetic rats. Invest. Ophthalmol. Vis. Sci. *39*, 2190–2194.

62. Roy, S., Kern, T.S., Song, B., and Stuebe, C. (2017). Mechanistic Insights into Pathological Changes in the Diabetic Retina: Implications for Targeting Diabetic Retinopathy. Am. J. Pathol. *187*, 9–19.

63. Rubsam, A., Parikh, S., and Fort, P.E. (2018). Role of Inflammation in Diabetic Retinopathy. Int. J. Mol. Sci. *19*, 583687.

64. Wang, J., Xu, X., Elliott, M.H., Zhu, M., and Le, Y.Z. (2010). Muller cell-derived VEGF is essential for diabetes-induced retinal inflammation and vascular leakage. Diabetes *59*, 2297–2305.

65. Yuuki, T., Kanda, T., Kimura, Y., Kotajima, N., Tamura, J., Kobayashi, I., and Kishi, S. (2001). Inflammatory cytokines in vitreous fluid and serum of patients with diabetic vitreoretinopathy. J. Diabetes Complications *15*, 257–259.

66. Bogan, J.S. (2022). Ubiquitin-like processing of TUG proteins as a mechanism to regulate glucose uptake and energy metabolism in fat and muscle. Front. Endocrinol. *13*, 1019405.

67. Xu, H., Czerwinski, P., Hortmann, M., Sohn, H.Y., Förstermann, U., and Li, H. (2008). Protein kinase C alpha promotes angiogenic activity of human endothelial cells via induction of vascular endothelial growth factor. Cardiovasc. Res. *78*, 349–355.

68. Alagorie, A.R., Nassisi, M., Verma, A., Nittala, M., Corradetti, G., Velaga, S., and Sadda, S.R. (2020). Relationship between proximity of choriocapillaris flow deficits and enlargement rate of geographic atrophy. Graefes Arch. Clin. Exp. Ophthalmol. *258*, 995–1003.

69. Nassisi, M., Tepelus, T., Corradetti, G., and Sadda, S.R. (2021). Relationship Between Choriocapillaris Flow and Scotopic Microperimetry in Early and Intermediate Age-related Macular Degeneration. Am. J. Ophthalmol. *222*, 302–309.

70. Ratnapriya, R., and Chew, E.Y. (2013). Age-related macular degeneration-clinical review and genetics update. Clin. Genet. *84*, 160–166.

71. Tiosano, L., Corradetti, G., and Sadda, S.R. (2021). Progression of choriocapillaris flow deficits in clinically stable intermediate age-related macular degeneration. Eye (Lond) *35*, 2991–2998.

72. Goldeman, C., Ozgür, B., and Brodin, B. (2020). Culture-induced changes in mRNA expression levels of efflux and SLC-transporters in brain endothelial cells. Fluids Barriers CNS *17*, 32.

73. He, Y., Yao, Y., Tsirka, S.E., and Cao, Y. (2014). Cell-culture models of the blood-brain barrier. Stroke *45*, 2514–2526.

74. Kim, S.A., Kim, S.J., Choi, Y.A., Yoon, H.J., Kim, A., and Lee, J. (2020). Retinal VEGFA maintains the ultrastructure and function of choriocapillaris by preserving the endothelial PLVAP. Biochem. Biophys. Res. Commun. *522*, 240–246.

75. Saint-Geniez, M., Maldonado, A.E., and D'Amore, P.A. (2006). VEGF expression and receptor activation in the choroid during development and in the adult. Invest. Ophthalmol. Vis. Sci. *47*, 3135–3142.

76. Wang, Y., Sabbagh, M.F., Gu, X., Rattner, A., Williams, J., and Nathans, J. (2019). Beta-catenin signaling regulates barrier-specific gene expression in circumventricular organ and ocular vasculatures. Elife *8*, e43257.

77. Benz, F., Wichitnaowarat, V., Lehmann, M., Germano, R.F., Mihova, D., Macas, J., Adams, R.H., Taketo, M.M., Plate, K.H., Guerit, S., et al. (2019). Low wnt/beta-catenin signaling determines leaky vessels in the subfornical organ and affects water homeostasis in mice. Elife *8*, e43818.

78. Cho, C., Smallwood, P.M., and Nathans, J. (2017). Reck and Gpr124 Are Essential Receptor Cofactors for Wnt7a/Wnt7b-Specific Signaling in Mammalian CNS Angiogenesis and Blood-Brain Barrier Regulation. Neuron *95*, 1056–1073.e5.

79. Wang, Y., Rattner, A., Zhou, Y., Williams, J., Smallwood, P.M., and Nathans, J. (2012). Norrin/Frizzled4 Signaling in Retinal Vascular Development and Blood Brain Barrier Plasticity. Cell *151*, 1332–1344.

80. Munji, R.N., Soung, A.L., Weiner, G.A., Sohet, F., Semple, B.D., Trivedi, A., Gimlin, K., Kotoda, M., Korai, M., Aydin, S., et al. (2019). Profiling the mouse brain endothelial transcriptome in health and disease models reveals a core blood-brain barrier dysfunction module. Nat. Neurosci. *22*, 1892–1902.

81. Kalucka, J., de Rooij, L.P.M.H., Goveia, J., Rohlenova, K., Dumas, S.J., Meta, E., Conchinha, N.V., Taverna, F., Teuwen, L.A., Veys, K., et al. (2020). Single-Cell Transcriptome Atlas of Murine Endothelial Cells. Cell *180*, 764–779.e20.

82. Markowitz, D., Goff, S., and Bank, A. (1988). A safe packaging line for gene transfer: separating viral genes on two different plasmids. J. Virol. *62*, 1120–1124.

83. Li, H. (2021). New strategies to improve minimap2 alignment accuracy. Bioinformatics *37*, 4572–4574.

84. Ying, C., Göke, J., Sim, A., Wan, Y.K., Turaga, N., and Love, M. (2021). GoekeLab/bambu: bambu v2.0.0-Bioconductor release (Zenodo).

85. Love, M.I., Huber, W., and Anders, S. (2014). Moderated estimation of fold change and dispersion for RNA-seq data with DESeq2. Genome Biol. *15*, 550.

86. Stephens, M. (2017). False discovery rates: a new deal. Biostatistics *18*, 275–294.

87. Gu, Z., Eils, R., and Schlesner, M. (2016). Complex heatmaps reveal patterns and correlations in multidimensional genomic data. Bioinformatics *32*, 2847–2849.

88. Kiefer, F., Anhauser, I., Soriano, P., Aguzzi, A., Courtneidge, S.A., and Wagner, E.F. (1994). Endothelial cell transformation by polyomavirus middle T antigen in mice lacking Src-related kinases. Curr. Biol. *4*, 100–109.

89. Baghirova, S., Hughes, B.G., Hendzel, M.J., and Schulz, R. (2015). Sequential fractionation and isolation of subcellular proteins from tissue or cultured cells. MethodsX *2*, 440–445.

## STAR★METHODS

### KEY RESOURCES TABLE

| REAGENT or RESOURCE | SOURCE | IDENTIFIER |
|---|---|---|
| **Antibodies** | | |
| armenian hamster anti-PECAM1/CD31 | Sigma/Merck | Cat# MAB1398Z; RRID:AB_94207 |
| rabbit anti-CLDN5 | ThermoFisher Scientific | Cat# 34–1600; RRID:AB_2533157 |
| rabbit anti-αSMA/ACTA2 | Abcam | Cat# ab5694; RRID:AB_2223021 |
| rat anti-PLVAP | BD Biosciences | Cat# 553849; RRID:AB_395086 |
| rat anti-TJP1 | ThermoFisher Scientific | Cat# 14-9776-82; RRID:AB_2573026 |
| mouse anti β-actin | Sigma/Merck | Cat# A1978; RRID:AB_476692 |
| rabbit anti non-phospho (active) β-Catenin (Ser45) | Cell Signaling Technologies | Cat# 19807; RRID:AB_2650576 |
| goat anti-armenian hamster IgG-AF488 | Jackson ImmunoResearch | Cat# 127-545-160; RRID:AB_2338997 |
| goat anti-rabbit IgG-Cy3 | Jackson ImmunoResearch | Cat# 111-165-003; RRID:AB_2338000 |
| goat anti-rat IgG-AF488 | Jackson ImmunoResearch | Cat# 112-545-143; RRID:AB_2338361 |
| goat anti-rabbit HRP (horseradish peroxidase) | Dako/Agilent Technologies | Cat# P0448; RRID:AB_2617138 |
| goat anti-mouse HRP (horseradish peroxidase) | Jackson ImmunoResearch Labs | Cat# 115-035-068 RRID:AB_2338505 |
| **Biological samples** | | |
| Total RNA samples of Mus musculus: Brain Endothelial cells (BEC) | This paper | N/A |
| Total RNA samples of Mus musculus: Choroideal Endothelial cells (ChEC) | This paper | N/A |
| Total RNA samples of Mus musculus: Retinal Endothelial cells (REC) | This paper | N/A |
| Cytosolic protein extracts of Mus musculus: Brain Endothelial cells (BEC) | This paper | N/A |
| Cytosolic protein extracts of Mus musculus: Choroideal Endothelial cells (ChEC) | This paper | N/A |
| Cytosolic protein extracts of Mus musculus: Brain Endothelial cells (BEC) | This paper | N/A |
| **Chemicals, peptides, and recombinant proteins** | | |
| Gibco™ Puromycin-Dihydrochlorid | Fisher Scientific | Cat# A1113803 |
| Bovine Serum Albumin Fraction V pH 5.2 | Sigma/Merck | Cat# 810533 |
| Collagenase type 4 | Worthington Biochemical | Cat# LS004188 |
| Neutral protease (Dispase) | Worthington Biochemical | Cat# LS02104 |
| Deoxyribonuclease I | Worthington Biochemical | Cat# LS006342 |
| Recombinant murine VEGF165 | Peprotech | Cat# 450-32 |
| Fibronectin bovine plasma | Sigma/Merck | Cat# F1141 |
| Polybrene Transfection Reagent | EMD Milipore → Sigma/Merck | Cat# TR-1003-G |
| Normal goat serum | Thermo Fisher Scientific | Cat# 31872 |

(*Continued on next page*)

*Continued*

| REAGENT or RESOURCE | SOURCE | IDENTIFIER |
|---|---|---|
| 4′,6-Diamidin-2-phenylindol (DAPI) | Sigma/Merck | Cat# 10236276001 |
| Mowiol 4–88/DABCO mounting medium | | |
| RNaseOUT™ Ribonuclease inhibitor | Thermo Fisher Scientific | Cat# 10777019 |
| Maxima H Minus Reverse Transkriptase 200u/μL | Thermo Fisher Scientific | Cat# EP0751 |
| RNAse Cocktail™ Enzyme Mix | Thermo Fisher Scientific | Cat# AM2286 |
| LongAmp® Taq 2X Master Mix | New England Biolabs | Cat# M0287L |
| Blunt/TA Ligase Master Mix | New England Biolabs | Cat# M0367L |
| CHIR99021 | Sigma/Merck | Cat# SML1046 |
| Sodium fluorescein | | |
| Digitonin-used as non-ionic detergent | Sigma/Merck | Cat# D141 |
| Halt™ Protease-Inhibitor-Cocktail (100x) | Thermo Fisher Scientific | Cat# 87786 |
| PhosSTOP™ Phosphatase-Inhibitor Mix | Sigma/Merck | Cat# 4906845001 |
| cOmplete™ Protease Inhibitor Cocktail | Sigma/Merck | Cat# 11697498001 |
| **Critical commercial assays** | | |
| Pierce™ BCA Protein Assay Kit | Thermo Fisher Scientific | Cat# 23225 |
| RNeasy Plus Mini Kit | QIAGEN | Cat# 74136 |
| (Nanopore) Direct cDNA sequencing kit | Oxford Nanopore Technologies | Cat# SQK-DCS109 |
| NEBNext® Ultra™ II End Repair/dA-Tailing Module | New England Biolabs | Cat# E7546L |
| NEBNext® Quick Ligation Module | New England Biolabs | Cat# E6056L |
| Flow Cell Priming Kit | Oxford Nanopore Technologies | Cat# EXP-FLP002 |
| Flow Cell Wash Kit | Oxford Nanopore Technologies | Cat# EXP-WSH-004 |
| SuperSignal™ West Pico PLUS Chemiluminescence substrate | Thermo Fisher Scientific | Cat# 34579 |
| **Deposited data** | | |
| Raw and analyzed Nanopore sequencing data | This paper | www.ncbi.nlm.nih.gov/geo Accession number GSE254272 |
| Genome assembly GRCm39 | NCBI National Center for Biotechnology Information | GCF_000001635.27 |
| RNA-sequencing raw and analyzed data mouse EC | Kalucka et al.[81]; https://doi.org/10.1016/j.cell.2020.01.015 | ArrayExpress: E-MTAB-8077 |
| **Experimental models: Cell lines** | | |
| Mus musculus: GPE-Neo stably transfected packaging cell line GP + E−86 | Britta Engelhard, Theodor Kocher Institute, University of Bern | Markowitz et al.[82] https://doi.org/10.1128/JVI.62.4.1120-1124.1988. |
| Mus musculus: Brain Endothelial cells (BEC) | This paper | N/A |
| Mus musculus: Choroideal Endothelial cells (ChEC) | This paper | N/A |
| Mus musculus: Retinal Endothelial cells (REC) | This paper | N/A |
| **Experimental models: Organisms/strains** | | |
| Mus musculus: Strain 129/Sv wildtype | | APB ID: 4898 |
| **Software and algorithms** | | |
| GraphPad Prism v 10.2.3 | GraphPad | https://www.graphpad.com/ |
| Guppy basecalling software v6.1.3 | Oxford Nanopore Technologies | dna_r9.4.1_450bps_sup.cfg |
| ImageJ 1.53k | Wayne Rasband and contributors, National Institute of Health, USA | http://imagej.nih.gov/ij |
| Zen3.2 blue edition | Carl Zeiss | https://www.zeiss.com/microscopy |
| R v 4.2 | R-Project for statistical computing | https://www.r-project.org/ |
| minimap2 | | https://github.com/lh3/minimap2. |

(*Continued on next page*)

*Continued*

| REAGENT or RESOURCE | SOURCE | IDENTIFIER |
|---|---|---|
| | Li 2021[83]; https://doi.org/10.1093/bioinformatics/btab705 | |
| bambu v2.2.0 | Ying et al., 2021[84]; https://doi.org/10.5281/zenodo.3900024. | https://github.com/GoekeLab/bambu/tree/v2.0.0 |
| DESeq2 v1.36.0 | Love et al.[85]; https://doi.org/10.1186/s13059-014-0550-8 | http://www.bioconductor.org/packages/release/bioc/html/DESeq2.html. |
| Ashr | Stephens, 2017[86]; https://doi.org/10.1093/biostatistics/kxw041 | http://github.com/stephens999/ashr |
| Enrichr | maayanlab.cloud | https://maayanlab.cloud/Enrichr/ |
| Appyter gene set comparison tool | maayanlab.cloud | https://appyters.maayanlab.cloud/CompareSets/ |
| ComplexHeatmap v2.18.0 | Gu, Eils, & Schlesner, 2016[87]; https://doi.org/10.1093/bioinformatics/btw313 | http://www.bioconductor.org/packages/devel/bioc/html/ComplexHeatmap.html |
| Other | | |
| Nunc™ Lab-Tek™ 8 well Chamber Slide System | ThermoFisher Scientific | 177402 |
| AMPure XP beads | Beckman Coulter | A63881 |
| MinION and GridION Flow Cell (R.9.4.1) | Oxford Nanopore Technologies | FLO-MIN106D |
| Corning® Transwell® polyester membrane cell culture inserts | Fisher Scientific | 10565482 |
| 4–15% Mini-PROTEAN® TGX™ Precast Protein Gels, 12-well, 20 μL | BioRAD | 4561085 |

## EXPERIMENTAL MODEL AND STUDY PARTICIPANT DETAILS

### Mice

The mouse line 129/Sv served as the primary tissue donor for the generated cell culture models. For generation of REC postnatal day (P) 30 mice and for ChEC and BEC P15 mice of both sexes were used. All procedures of animal handling conformed to the Uniform Requirements for manuscripts submitted to biomedical journals, the tenets of the National Institutes of Health Guidelines on the Care and Use of Animals in Research, the EU Directive 2010/63/E) and the German government. We furthermore followed institutional guidelines. Removal of brains and eyes were approved by the Government of Bavaria, Regierung von Unterfranken, Würzburg and city of Hamburg, Germany (ORG_1126).

### Immortalization and endothelial cell culture

All cell lines, used in this paper, were cultured in Dulbecco's Modified Eagle Medium (DMEM) + 10% fetal calf serum +10μg/ml gentamicin (ThermoFisher Scientific). The cells were incubated at 37°C and 5% $CO_2$ and visually inspected every 2–3 days for bacterial or fungal contamination. For generation of REC eight P30 mice, for ChEC seven P15 mice, and for BEC five P15 mice of both sexes were used. BEC were isolated and immortalized as previously described.[15,17,18,20] For isolation of REC and ChEC, mice were euthanized, eyes enucleated with blunt microsurgical forceps, and transferred to ice-cold sterile PBS. Ocular tissues were dissected using a stereomicroscope. Briefly, the cornea was penetrated centrally with a narrow-gauge needle and opened by making crosswise incisions with microsurgical scissors. Using blunt microsurgical forceps, the lens and vitreous body were streaked out gently through the opening and discarded. Neuroretinae (retinae without RPE) were dissected similarly by using slightly more pressure and transferred to ice-cold sterile PBS. After removal of the neuroretinae, the choroids (and RPE) were scraped of the sclera using blunt microsurgical forceps and transferred to ice-cold sterile PBS. The collected tissue was pelleted at 400 g, 4°C for 3 min, the supernatant aspirated, and the tissue resuspended in DMEM/25 mM HEPES +150 U/ml collagenase, type 4 (Worthington Biochemical, LS004188)) + 1 U/ml neutral protease (Worthington Biochemical, LS02104) + 5 U/ml DNase I (Worthington Biochemical, LS006342) by triturating with a 200 μL pipette tip (100 μL per retina/choroid). Tissues were incubated at 37°C for 5 min (retina) or 10–15 min (choroid) and the suspensions triturated again until no more clumps were visible. Enzymes were quenched by adding 20% FCS, cells pelleted at 400 g,

4°C for 3 min, the supernatant discarded, and the cell pellet resuspended in 5 mL ice-cold PBS/1% BSA. Cell suspension was passed through a 40 μm cell strainer, cells were washed once with ice-cold PBS/1% BSA and resuspended in cell culture medium supplemented with 10 ng/mL VEGF165 (Peprotech, 450-32). Cells were seeded into four (retina) or eight (choroid) wells of a fibronectin-coated (Merck, F1141) 48-well plate and incubated for 24h. The polyoma virus middle T antigen was used to selectively immortalize endothelial cells in primary cultures of mouse retinal or choroidal cells. Regarding immortalization using the polyomavirus middle T antigen a single rate-limiting step has been found to induce selectively endothelial tumors (hemangiomas) in mice. In particular, the authors[88] demonstrated that the activation of Src-like kinases is an important component of polyomavirus middle T antigen-induced transformation of endothelial cells.

Upon transduction with the middle T antigen, the mixed cell cultures gradually became endothelial monocultures. Since only endothelial cells were immortalized, all contaminating non-endothelial cells ceased proliferating upon reaching the Hayflick limit and were diluted out by continuous passaging. By day 60, no more non-endothelial cells were detectable in our cultures. Middle T antigen-encoding retrovirus was obtained from conditioned medium of GPEmTneo cells. GPEmTneo cells were kindly provided by Britta Engelhard, Theodor Kocher Institute, University of Bern, Bern, Switzerland. These cells derive from the retroviral packaging cell line GP + E−86[82] stably transfected with the retroviral vector N-TKmT.[24] GPEmTneo cells were maintained in gelatin-coated culture vessels and splitted in a 1:5 ratio on a routine base (approximately every 5–6 days). GPEmTneo culture medium was conditioned for 2–3 days until the cells reached 100% confluence. Harvested conditioned medium was passed through 0.45 μm pore size syringe filters and used right away or stored at −80°C. After 24 h the non-attached, dead endothelial cells were washed off with PBS and conditioned medium from GPEmTneo cells, supplemented with 8 μg/mL polybrene (EMD Milipore, Burlington, USA, purchased from Sigma/Merck, TR-1003-G), was added for middle T antigen transduction. Cells were incubated for 24h and transduction was repeated with fresh conditioned medium + polybrene for another 24h. Transduction medium was replaced with fresh culture medium and cells were maintained at passage 0 until clones of immortalized endothelial cells became visible, which occurred before (retina) or after (choroid) reaching confluence. Cells were trypsinized, pooled, and seeded into larger culture vessels. Once the cells had expanded to confluence in T75 flasks, they were split at a 1:4 ratio. Medium was changed twice a week. By day 60 of culture, endothelial cells had completely outgrown other cell types and cultures represented endothelial monocultures.

### Ethics approval and consent to participate

All procedures conformed to the Uniform Requirements for manuscripts submitted to biomedical journals, the tenets of the National Institutes of Health Guidelines on the Care and Use of Animals in Research, the EU Directive 2010/63/E).

## METHOD DETAILS

### Immunofluorescence staining

5 x $10^4$ cells per chamber were seeded into fibronectin-coated (Merck, F1141) 8-chamber slides (ThermoFisher Scientific, 177402) and incubated until confluent. To examine the effect of WNT/β-catenin activation, cells were incubated with medium containing 10μM CHIR99021 (Merck, SML1046) or control medium for 7 days. Medium was aspirated and cells were fixed with 4% paraformaldehyde (PFA) in PBS for 15 min at room temperature. Chambers were removed leaving only the silicone sealing behind. Cells were washed three times for 5 min with PBS and blocked/permeabilized with PBS/5% normal goat serum/0.3% Triton X-100. Cells were incubated with 5 μg/mL armenian hamster anti-PECAM1/CD31 (Merck, MAB1398Z), 2.5 μg/mL rabbit anti-CLDN5 (ThermoFisher Scientific, 34–1600), 2 μg/mL rabbit anti-αSMA/ACTA2 (Abcam, ab5694), 5 μg/mL rat anti-PLVAP (BD Biosciences, 553849), and/or 5 μg/mL rat anti-TJP1 (ThermoFisher Scientific, 14-9776-82) in PBS/1% bovine serum antigen (BSA)/0.3% Triton X-100 at 4°C overnight. Cells were washed as mentioned above and incubated with goat anti-armenian hamster IgG-AF488 (Jackson ImmunoResearch, 127-545-160), goat anti-rabbit IgG-Cy3 (Jackson ImmunoResearch, 111-165-003), and/or goat anti-rat IgG-AF488 (Jackson ImmunoResearch, 112-545-143) diluted 1:1000 in PBS/1% BSA/0.3% Triton X-100/1 μM DAPI for 1h. Again, cells were washed as mentioned above, the silicone sealing removed, and a coverslip mounted using Mowiol 4–88/DABCO mounting medium. Cells were imaged using the Axio Imager.M2 with Apotome.2 (Carl Zeiss Microscopy, Oberkochen, Germany). The ZEN interactive analysis tool was used to count the nuclei and determine the stained area of the respective antibodies (CLD5, TJP1 or PLVAP). The measured area was normalized to the number of nuclei. Statistical analysis was performed with GraphPad Prism v 10.2.3 (https://www.graphpad.com/).

### Third generation long-range RNA sequencing (nanopore)

Cells from passage 9 (ChEC) and 10 (REC/BEC) were seeded in triplicates into T75 flasks and incubated until confluent. Cells were washed once with PBS and total RNA was isolated using the RNeasy Plus Mini Kit (QIAGEN, Hilden, Germany) according to the manufacturer's instructions. RNA quality was determined using the Bioanalyzer 2100 (Agilent Technologies, Santa Clara, CA). All samples had a RIN ≥9.5. 10 μg total RNA for each sample were used for library preparation with the Nanopore Direct cDNA sequencing kit (#SQK-DCS109, Oxford Nanopore Technologies) with native barcode expansions (#EXP-NBD104, ONT) according to manufacturer's protocol (version: DCB_9091_v109_revL_14Aug2019). First, cDNA was synthesized. The ONT primer VNP was incubated for 5 min together with the RNA and dNTPs at 65°C and then snap cooled on a pre-chilled block. Afterward the SSP primer, 5x RT Buffer (supplied with reverse transcriptase) and RNaseOUT (#10777019, Thermo Fisher) were added, the samples were mixed

by flicking and incubated for 2 min at 42°C. Maxima H Minus RT (#EP0753, Thermo Fisher Scientific) was added, samples were mixed and incubated for 90 min at 42°C, 5 min at 85°C and were then cooled to 4°C. RNA was digested for 10 min with RNAse Cocktail Enzyme Mix (#AM2286, Thermo Fisher Scientific) at 37°C followed by cleanup of the samples using AMPure XP beads (#A63881, Beckman Coulter) according to ONT protocol. The eluted cDNA was used for 2nd strand synthesis. To this end, PR2 primer and 2X LongAmp Taq Master Mix (#M0287L, NEB) were mixed with the cDNA samples and incubated for 1 min at 98°C, 1 min at 50°C and 15 min at 65°C. The double stranded DNA was cleaned up with AMPure XP beads and taken forward to end preparation with the NEBNext Ultra II End Repair/dA-Tailing Module (#E7546L, NEB). After bead cleanup, native barcode ligation was performed. Each sample was labeled with a single assigned barcode by incubation of the sample together with the barcode and Blunt/TA Ligase Master Mix (#M0367L, NEB) for 10 min at 21°C. After another cleanup step, samples were eluted in 21.7 μL nuclease-free water and pooled. 65 μL of the pooled sample were directly used for adapter ligation, the remaining sample was stored at −20°C. The adapter mix II was ligated to the sample using the NEBNext Quick Ligation Module (#E6056L, NEB) for 10 min at 21°C. During the following bead cleanup, the library was washed with short fragment buffer and eluted in 12 μL elution buffer. Before sequencing the flow cell (#FLO-MIN106D, ONT) was checked and primed (#EXP-FLP002, ONT) according to manufacturer's protocol. The library was mixed with sequencing buffer and loading beads and was dropwise added into the sequencing port of the flow cell. Sequencing was performed on a MinION Mk1C (MinKNOW v22.03.4) for 72 h. After 24- and 48-h sequencing was paused to wash the flow cell using the Flow Cell Wash Kit (#EXP-WSH-004, ONT). To maximize output, 65 μL of stored sample was subjected to adapter ligation and reloaded to the washed and primed flow cell. Basecalling and demultiplexing was performed using the Guppy basecalling software v6.1.3 with the SUP profile (dna_r9.4.1_450bps_sup.cfg).

### Bioinformatics

An average of approx. 500,000 full-length reads were analyzed per sample. The reads were aligned against gencode mus musculus version vM29 (GRCm39) using minimap2.[83] All subsequent analyses were conducted in R v4.2. Samples were screened for outliers using PCA and clustering analysis; no outliers were detected. Reads were quantified using bambu v2.2.0.[84] Transcriptional dysregulation was computed using DESeq2 v1.36.0[85] with the tissue origin of the endothelial cells as the variable of interest and using ashr[86] as the fold change shrinkage estimator. The Benjamini-Hochberg procedure was used to correct for multiple comparisons ($p$-adjusted; $p_{adj}$). The four clusters of differentially expressed genes were subjected to gene enrichment analyses for signaling pathways, gene ontologies, and transcriptional regulators using the Enrichr online tool (https://maayanlab.cloud/Enrichr/). Furthermore, the clusters were analyzed for overlaps with tissue-specific endothelial subtype markers using the Appyter gene set comparison tool (https://appyters.maayanlab.cloud/CompareSets/). Tissue-specific endothelial subtype marker gene sets were retrieved from the single cell transcriptome atlas of murine endothelial cells.[81] Heatmaps and k-mer analysis was carried out using ComplexHeatmap v2.18.0.[87] Scripts are available upon reasonable request.

### Western Blot of active β-catenin and PLVAP

2 x $10^5$ cells were seeded in biological triplicates into tissue culture treated 6 well plates (9,6$cm^2$ growth area) and incubated until the cells reached 100% confluency. In accordance to the Permeability assay cells were incubated with medium containing 10μM CHIR99021 (Merck, SML1046) or control medium for 7 days. To observe accumulation of active non-phosphorylated β-catenin in the cytoplasm as a hallmark of WNT/β-catenin pathway activity, we harvested only the cytoplasmic fraction of the endothelial cells to avoid contamination with plasma-membrane associated β-catenin. We used a protocol based on[89] that uses a Digitonin based cell lysis buffer and modified it to harvest cytosolic proteins during tissue culture. After 7 days of incubation, the cells were generously washed with cold PBS. The lysis buffer (150mM NaCl, 50mM HEPES pH 7.4, 25μg/mL Digitonin (Merck/Sigma D141), 1M Hexylene glycol) was freshly supplemented with 1% Halt Protease-Inhibitor-Cocktail (100x) (Thermo Fisher Scientific, 87786) and PhosStop Phosphatase inhibitor (Merck/Sigma, 4906845001). Each well-plate received 400μL of lysis buffer per well and was stored at 4°C for 10 min under constant agitation. The lysis buffer was harvested and traces of cells or cellular debris removed by centrifugation. Proteins were precipitated from lysis buffer with 125μg/ml Sodium-deoxycholate (NaDOC) and 6% trichloroacetic acid TCA. Precipitated protein pellets were washed with cold acetone and resuspended in 100μL 1xTris-buffered saline (TBS) + 2%SDS. To facilitate resuspension of the precipitated protein pellets in TBS, the samples were heated to 95°C under constant agitation for 10–15 min. The protein yield was quantified with the Pierce BCA Protein Assay Kit (#23225, Thermo Fisher Scientific) according to manufacturers instruction. Based on quantification of the protein yield, all samples were adjusted to 0,375μg/ml protein and supplemented with 4x Laemmli Buffer (BioRAD, 1610747) and 50mM DTT (final concentration). For quantification of PLVAP samples containing the complete cellular proteome were analyzed. Again, the cells were treated with 10μM CHIR99201 or control medium for 7 days respectively, washed thoroughly with PBS and harvested in **R**adio-**I**mmuno**p**recipitation-**a**ssay (RIPA) buffer (25mM Tris, 150mM NaCl, 1% TritonTx-100, 0.5% Sodium-deoxycholate, 0.1% SDS +1 tablet/10mL Roche cOmplete Protease-Inhibitor (Merck, 11697498001)). Cells were harvested via scraping in a minimal amount of RIPA buffer (~70μL per 6 well) and lysed by repeated vortexing on ice over 30 min. Cellular debris was removed from the protein lysate via centrifugation at 17.000g/4°C/10min. After quantification of the protein yield with the Pierce BCA Protein Assay Kit, samples were adjusted to 2 mg/ml and supplemented with 4X Laemmli Buffer +50mMDTT accordingly. Protein samples were resolved by a 4–15% SDS-polaycrylamide gradient gel (BioRAD, 4561085) and transferred on a polyvinylidene fluoride membrane. The membrane was blocked with 5% nonfat dried milk powder in 1xTBS+ 0.1% Tween 20 (TBST) for 1 h at room temperature under constant agitation. After the blocking procedure, the membrane

was sliced in half and incubated with the corresponding primary antibody, diluted in 5%BSA in TBST (Non-phosphorylated β-catenin; PLVAP 1:1000 ratio) or 5% nonfat dried milk powder in TBST(β-actin; 1:10.000 ratio). Membranes were incubated overnight at 4°C under constant agitation. Membranes were washed with TBST 3 times for 10 min each and incubated with the corresponding secondary antibody. Secondary antibodies were diluted in 5% nonfat dried milk powder in TBST at a ratio of 1:10.000 and generously poured on the membranes to completely cover them. Incubation with secondary antibody was done at RT under constant agitation. After secondary antibody incubation the membranes were washed again with TBST 3 times. Western Blot Luminescence signals were evaluated with SuperSignal West Pico PLUS Chemiluminescence substrate (Thermo Fisher Scientific, 34579) using the Fusion Solo System (Vilber Lourmat). Luminescence images were evaluated using ImageJ 1.53k (http://imagej.nih.gov/ij). The intensity of non-phosphorylated β-catenin or PLVAP were measured and normalized against the corresponding β-actin band intensity. Statistical analysis was performed with GraphPad Prism v 10.2.3 (https://www.graphpad.com/).

### Permeability assay

5 x $10^4$ cells were seeded in triplicates into transwell inserts (1.12 $cm^2$ growth area, 0.4 μm pore size, Fisher Scientific, 10565482) fitted into 12-well plates (top chamber: 0.5 mL medium, bottom chamber: 1.5 mL medium) and incubated until the cells were confluent. Once confluent, cells were stimulated for 7days with 10 μM CHIR99021 (Merck, SML1046) or solvent only (DMSO). Medium was switched to normal culture medium and cells were incubated for 1h. 10 μM sodium fluorescein (Alcon, Freiburg, Germany) was added to the upper chambers and samples (150 μL) were taken after 15, 30, 45, and 60 min from the lower chambers, transferred to a 96-well plate, and replaced with 150 μL pre-warmed, fresh medium. After sample acquisition, additional triplicate wells of the 96-well plate were filled with 150 μL medium +1 μM sodium fluorescein (fluorescein in upper chamber at t = 0, 1:10 dilution) or 150 μL medium only (background fluorescence). Relative fluorescence units (RFU) of the samples and controls were measured using a microtiter plate reader. RFU were corrected for background fluorescence and dilutions. Fluorescein volume flux (V) in μl was calculated using the formula: V(t) = RFU(t) x 1500 μL/RFU(t = 0). Fluorescein permeability coefficients (P) in cm/s for the cell monolayers were calculated using the volume flux slopes (m = V(t)/t) corrected for the permeability of the insert filters (m(cells) = 1/[1/m(cells+filter) - 1/m(filter)]) and the formula P = m(cells)/1000/1.12 $cm^2$/60 s.

## QUANTIFICATION AND STATISTICAL ANALYSIS

The Benjamini-Hochberg adjustment was used to correct nanopore RNAsequencing comparisons for multiple testing. One-way ANOVA was used for statistical evaluation of the densitometric analyses of the β-catenin/PLVAP western blots. two-way ANOVA was used for permeability coefficients. An unpaired t test with Welch correction was used for quantification of the immunofluorescence signals. $p$ values <0.05 were considered to be statistically significant and marked (*) accordingly.

For cell culture experiments, each new seeding was considered a biological replicate (n). All data are shown as mean ± SD, or mean ± SEM (normalized counts), respectively.